Department of Mechanical and
Industrial Engineering
University of Illinois at
Urbana-Champaign
Urbana, IL 61801

ORNL/SUB/85-55904/01
UILU ENG-88-4011

DEVELOPMENT OF A DESIGN METHODOLOGY FOR HIGH-TEMPERATURE CYCLIC APPLICATION OF MATERIALS WHICH EXPERIENCE CYCLIC SOFTENING

F. A. Leckie, D. L. Marriott, J. F. Stubbins,
J. L. Handrock, and B. Kschinka

A Technical Report Prepared for

OAK RIDGE NATIONAL LABORATORY
Oak Ridge, TN 37831

Operated by

MARTIN MARIETTA ENERGY SYSTEMS, INC.
for the
U.S. DEPARTMENT OF ENERGY

Under

Contract DE-AC05-840R21400

August 1987

Printed in the United States of America. Available from
National Technical Information Service
U.S. Department of Commerce
5285 Port Royal Road, Springfield, Virginia 22161
NTIS price codes—Printed Copy: A04 Microfiche A01

ORNL/Sub--85-55904/1

DE90 001585

Report Prepared by

F. A. Leckie, D. L. Marriott, J. F. Stubbins
J. L. Handrock, B. Kschinka

University of Illinois at Urbana-Champaign

under

Contract 19X55904

for

OAK RIDGE NATIONAL LABORATORY
Oak Ridge, Tennessee 37831
operated by
MARTIN MARIETTA ENERGY SYSTEMS, INC.
for the
U.S. DEPARTMENT OF ENERGY
under Contract DE-AC05-840R21400

Research sponsored by the U.S. Department of Energy, AR&TD Fossil Energy Materials Program, DOE/FE AA 15 10 10 0, Work Breakdown Structure Element UI-2.

ORNL/SUB/85-55904/01

University of Illinois

DEVELOPMENT OF A DESIGN METHODOLOGY FOR HIGH-TEMPERATURE CYCLIC APPLICATION OF MATERIALS WHICH EXPERIENCE CYCLIC SOFTENING

by

F. A. Leckie, D. L. Marriott, J. F. Stubbins
J. L. Handrock, B. Kschinka

University of Illinois at Urbana-Champaign

AUGUST 1987

Research sponsored by
U.S. Department of Energy,
Advanced Research and Technology Development
Fossil Energy Materials Program

Prepared by
D. L. Marriott, Mechanical Engineering Department
and
J. F. Stubbins, Nuclear Engineering Department
University of Illinois
1206 West Green Street
Urbana, IL 61801

under

Subcontract No. 19X55904

for

OAK RIDGE NATIONAL LABORATORY
Oak Ridge, Tennessee 37831
operated by
MARTIN MARIETTA ENERGY SYSTEMS, INC.
for the
U.S. DEPARTMENT OF ENERGY
under Contract No. DE-AC05-840R21400

TABLE OF CONTENTS

Page No.

1. INTRODUCTION.....1

2. LOW ALLOY STEEL.....4

3. AUSTENITIC STEELS.....23

4. CONCLUSIONS.....24

5. FUTURE WORK.....26

REFERENCES.....28

1. INTRODUCTION

The original intent of this project was to investigate the strain induced softening observed in low alloy steels, quenched and tempered to produce a predominantly bainitic microstructure. The softening phenomenon is both significant and persistent. As much as 30% of the initial yield strength can be lost as a result of the cyclic plastic deformation accumulated in a few hundred cycles. In addition, monotonic strength is affected by plastic deformation. Its effect in a monotonic tensile test is to reduce the ratio of tensile strength to yield to near unity, while the ultimate tensile strength occurs at strains of as little as 0.5%, well within the strain ranges observed in high temperature service under thermal transients.

Strain induced softening has at least two implications for component strength. The first is that the limit strength, and hence the reserve of strength to resist upset conditions, and to allow for the normal variations of material quality and service loading, can be degraded to a point where the advantages of heat treatment are negated. Secondly, the attainment of peak strength at such low strains introduces the possibility of strain localization or instability and premature failure by a variety of strain controlled damage mechanisms.

The project described in this report has, as its beginning, two investigations, the first a study of the effect of material softening on the overall structural stability of complex components, and the second an evaluation of damage induced through cyclic loads combined with high temperature environmental effects.

Component behavior in the presence of material softening has been investigated both theoretically and experimentally using notched bars of various acuities as the prototype "component". Experimental studies include creep, controlled strain rate and cyclic testing of notched specimens at high temperature (565°C). Theoretical work covers approximate methods of component analysis, and more detailed studies using finite element modeling, combined with simplified material constitutive models, to approximate the very complex action of strain induced softening.

Damage studies tended to focus on separating out the influences on fatigue of high temperature creep and oxidation. This was done by com-

paring cyclic performance in air and in vacuum, using a novel form of bellows encapsulation which avoided the need for expensive retorts.

The initial work was carried out on one grade of 2.25Cr 1Mo steel, with the intention of extending the investigation to other grades once the investigative techniques had been settled. In the interval between the beginning of the project and the present, however, considerable interest has grown in the application of modified forms of austenitic steel to very high temperature use in superheaters and reheaters. The ability to utilize these materials can mean an increase of 100°C in the top temperature in a power plant, which converts into a significant improvement in thermal efficiency for a very small investment in material. Given therefore that substantial economic advantage can be derived from substantiating the use of this class of material for high temperature operation, the direction of this project has been modified to continue on this class rather than the ferritic alloys originally under consideration.

The basic problem to be investigated in the austenitics is still essentially the same as that being addressed in the 2.25Cr 1Mo steels, that is, the concern for possible strength variations, either positive or negative, induced in the very complex microstructures by service conditions of cyclic load and high temperature. In changing to the new material the initial scope of the investigation has been increased firstly because so little is known about the cyclic behavior of these steels, so that it is uncertain at this time whether they will cyclically harden or soften. Secondly, their high temperature strength is obtained by a combination of extremely complex chemistry and thermomechanical working producing microstructures which are expected to age in service giving, as yet, unknown changes in resistance to either steady or cyclic load.

The direction to be taken in future work will therefore be a continuation of the experimental and theoretical program, using essentially the same types of specimens as employed for the ferritic alloys, but with higher temperatures, and possibly longer time scales to examine aging effects which were not noticeable in the ferritics.

So far work on the austenitic steels has been limited, due to availability, to a sample of 17Cr 14M CuMo stainless steel alloy. Progress at the time of writing is restricted to manufacture of test specimens, and some optical microscopy of the as-supplied material. Such results as have been obtained so far are reported in the latter sections of the report.

2. LOW ALLOY STEEL

2.1 Description of Materials and Equipment

Several CrMo low allow steels are currently being considered for pressure vessel construction in quench and tempered forms. While this provides a considerable enhancement of the monotonic strength characteristics, materials tested in this way suffer a significant loss of strength due to cyclic softening. In simple axial loading, this effect has been found to significantly reduce the long term creep strength, even when the stress range is well below the initial yield strength of the material. On this evidence alone it might be concluded that, where cyclic loading is expected, there may be little or no advantage in using the bainitic structured material in preference to the more common ferritic-pearlitic form. On the other hand, most practical instances of significant stress reversal in components only occur in localized regions such as notch details or surface layers in pipes under cyclic thermal gradients. It is therefore feasible to suppose that conditions may arise where local softening has an insignificant effect on the overall load carrying capacity of the component, thus allowing the full strength attained by heat treatment to be utilized in determining primary stress limits for design.

In order to explore the influence of cyclic softening on component load carrying capacity, a series of tests has been performed on plain and notched, axially loaded specimens. The object was to determine the relative effects of periodic load cycles on creep and tensile strength of the material alone as opposed to its response to complex strain reversals in which local behavior is kinematically constrained to some extent by the remainder of the structure.

An additional concern is the little-understood and potentially dangerous creep-fatigue damage interaction. Containment vessels typically start-up, shut-down, and experience fluctuations in operating conditions. Such cycles usually produce small mechanical strains, normally less than about 0.5 percent with hold periods ranging from perhaps 10 to 1000 hours throughout the design lifetime of 30 or 40 years [1]. These transients lead to a combination of creep and fatigue damage which is potentially more deleterious than either mechanism acting in-

dependently. Hence a component may fail in a relatively low number of such cycles, particularly in the presence of a hostile environment. The possibility of a premature failure therefore must be considered at temperatures where creep is likely to influence low cycle fatigue behavior. Accordingly, appropriate elevated temperature, strain-controlled fatigue data must be generated in the laboratory and extrapolated to anticipated service conditions. This work was undertaken to assess the sensitivity of bainitic 2.25Cr-1Mo steel to creep-fatigue-environment interactions for the purpose of high temperature structural design.

2.1.1 Material

The test material is a 2.25Cr-1Mo steel forging with low residuals manufactured by Kawasaki Steel (Heat 646363) and supplied by Oak Ridge National Laboratory. The composition is given in Table 1; note the low concentrations of P, S, As, Sn, and Sb impurities. The alloy was quenched and tempered in the form of 400 mm plate as follows: austenitize at 1070°C (1960°F) for 18 hours--water quench. Temper at 650°C (1200°F) for 17 hours--air cool. Follow with a simulated post-weld heat treatment at 695°C (1283°F) for 19 hours. This processing produced a microstructure consisting of essentially 100 percent bainite, as confirmed by microscopic analysis. Room temperature strengths fell within ASME SA336 Class F22 specifications. Complete tensile properties at room temperature and 565°C (1050°F) are given in Table 2.

2.1.2 Test Specimens

Three types of specimens were used in the deformation studies, the dimensions of which are given in Fig. 1.

The second two types of specimens consist of notched bars, the first of which contains a Bridgman notch with a moderate stress concentration factor (SCF) of 1.6. The second type of notch is a BS standard Vee-notch having a relatively high SCF of 4.4.

For environmental testing purposes, the plain section specimen shown in Fig. 2 was encapsulated. The unique double shoulder geometry was designed specifically for purposes of vacuum testing. The inner shoulders were provided to mount type 321 stainless steel flexible tub-

ing which acted as a miniature retort encapsulating the gage section of the specimen in vacuum. The tubing was fastened to the specimen shoulders using an electron-beam brazing process. The entire brazing procedure was performed in a vacuum of about 0.0013 Pa (10^{-5} torr). In this way the gage section of the specimen was encapsulated in a reasonable vacuum without resorting to a costly retort system. This technique also eliminated misalignment problems prevalent in complex retort arrangements. A vacuum-encapsulated specimen prepared in this manner is shown in Fig. 3. Complete details of this innovative technique are presented elsewhere [2].

The fatigue life of a component may be considered to be comprised of the nucleation of a crack and its subsequent propagation to a critical length. Dependent upon loading conditions, usually one mechanism or the other consumes the majority of useful life. In an effort to separate the relative amounts of crack initiation and crack growth, tiny notches were manufactured in selected specimens by the process of electro-discharge machining (EDM). Each notch specimen has four separate notches as depicted in Fig. 4. Notch dimensions were about 60 μm deep and 75 μm wide, with a notch root radius of roughly 40 μm to yield an elastic stress concentration factor of approximately 2.5. Two sets of notches were provided so that one set was available for microscopic analysis after failure occurred at the other set.

2.1.3 Mechanical Testing

Two test facilities were used. The uniaxial strain controlled fatigue tests were performed on a commercial closed-loop electro-hydraulic test machine equipped with a resistance furnace. A standard high temperature axial extensometer was employed to maintain strain control. Hysteresis loops were periodically recorded; the cyclic load imposed on the specimens was monitored on a strip chart recorder.

All tests were conducted at 565°C (1050°F) using a fully reversed strain range of 0.50 percent. This temperature, while above the anticipated service temperature of 482°C (900°F), was chose to enhance creep without altering the original carbide structure. The strain range was selected for three reasons. Firstly, it is a reasonable estimate of

anticipated service conditions. Secondly, there are currently fewer data at such strain levels than exist at 1.0 percent and above. Finally, previous research of annealed 2.25Cr-1Mo [3,4] found hold periods at low strain ranges to be more damaging than at higher strains (> 1%) relative to pure fatigue in each instance, suggesting a more sever creep-fatigue interaction effect.

Four basic strain histories were examined: pure fatigue (no hold periods), and fatigue with both tensile and compressive hold periods. These are shown schematically in Fig. 5. All hold periods were introduced at maximum absolute strain amplitude. Hold period duration was varied from 6 to 3 to 1.5 to 0.75 to 0.6 minutes. Strain rate during the ramp portions of the waveforms was 0.004 per second.

All specimens were used in the as-machined condition with no subsequent grinding or polishing. Failure was defined as a 50 percent reduction in tensile stress level from the initial (maximum) value.

Two 5-ton load capacity screw-driven electromechanical test machines manufactured to an ORNL mechanical design by Applied Test Systems, Inc. (ATS), provide the basis of the creep-fatigue testing performed in this study. The combined stepper-motor screw-jack driven features of this equipment produces low strain rate machine capable of producing strain rates from a maximum of 0.05%/s to as low as 6E-6%/hr. This capability allows the performance of creep-fatigue tests containing very slow ramp loadings and hold times of almost indefinite duration. This ability allows long term creep-fatigue tests to be completed which approach a more realistic representation of actual service conditions. For elevated temperature (up to 1000°C), these test frames are outfitted with three zone resistance split furnaces, each zone containing an independent temperature controller. Further details of the test equipment are given in Ref. 5.

2.2 Deformation Softening Studies

2.2.1 Description of Experimental Program

a) Basic Fatigue Test Results

Strain controlled fully reversed fatigue tests performed by Pejsa [6] show this material to experience significant cyclic softening. Tests were conducted on material in the as-received condition at 565°C for a variety of waveforms at total strain ranges of 0.5% and 1.0%. The softening behavior is a nearly continuous process from initial cycling right up to the point of failure. In all cases though, a significant portion of the softening occurs in the initial portion of the fatigue life.

From Pejsa's original data, it is possible to plot the maximum and minimum stress as a function of log cycles and strain range for each of the waveforms tested. Such a plot is shown in Fig. 6. for selected cyclic conditions. These results in effect represent the strength of the material under conditions of cyclic softening and will later be shown to correlate very well with load control tests performed on both plain and notched bars.

b) Constant Strain Rate Tests

Constant strain rate tensile tests have also been performed on smooth specimens to obtain elevated temperature strain rate effect data for this material under monotonic loading. For comparison room temperature tests (20°C) were completed at strain rates of 0.5%/min and 0.05%/min from 0 to 10% strain. Elevated temperature tests (565°C) were completed at strain rates of 0.5%/min, 0.05%/min, 0.005%/min, and 0.0005%/min. The stress versus strain data from these tests are plotted in Fig. 7. The room temperature tests showed essentially no strain rate effect. When tested at elevated temperatures (565°C) this material shows a much different stress-strain response. After reaching the 0.2% yield strength, the material experienced a small amount of hardening after which softening was observed. Not only was the amount of hardening very slight (maximum strength equal to 1.02 to 1.08 times the yield strength), the region over which hardening occurred was much less than that experienced at room temperature.

The elevated temperature tests also show significant strain rate effects. As strain rate increases, both the yield strength and the ultimate strength increase. Figure 7 shows that the rate of increase of the yield and ultimate strengths decreases slightly with increasing strain rate. After reaching the ultimate strength, the material softens at a rate which, to a first approximation, is insensitive to strain rate.

c) Periodic Load Reversals On Plain And Notched Bars

The phenomenon which focused this program on strain softening is the observation that low alloy steels in quenched and tempered form have been shown by Swindeman [7] to display considerable loss of creep endurance as a result of periodic load reversals even when the stress range is significantly lower than the initial yield stress range.

The effect of cyclic loading on strength is shown clearly by plotting the peak maximum and minimum stresses in strain controlled fatigue tests against the log cycles (see Fig. 6). Unlike the linear plots, these curves show no plateau, but instead a continuous, exponential decrease in strength with time. Cyclic strength appears to be strongly dependent on the frequency of the cycle but only weakly dependent on the wave shape of the strain history or the strain range. This suggests a simple first-order model of cyclic softening in which the current strength is represented as a function of the number of load cycles and the load cycle frequency $\sigma_y\ (N) = f_1(N) \cdot f_2(f)$ where N = number of load cycles and f = frequency in cycles/unit time.

To test the hypothesis, the uniaxial creep tests with interspersed load reversals have been plotted on the same graph as the softening curves in Fig. 8. These points fall close to the tensile stress softening line, and the specimen lives would be reasonably accurately predicted by simply assuming the strength to decrease with number of cycles until the tensile strength of the specimen is exceeded.

The same hypothesis holds for more complex stress situations. As also shown in Fig. 8, the lives of all notched specimens undergoing full load reversals are predicted quite well by the number of cycles required to reduce the cyclic strength to the effective stress at the notch net section at the specified cycle frequency.

The frequency dependence of cyclic strength can also be approximated relatively simply. The rate dependence of this material has been examined over a wide range of strain rates, and it is observed that the cycle-dependent softening curves for different frequencies vary in a way similar to the monotonic rate dependence. Figure 9 includes such a curve for a 1-hour cycle time, constructed theoretically on the above hypothesis, which corresponds very well with the one Bridgman specimen tested at that frequency.

From the results of fully reversed load tests on notched bars, it is clear that cyclic softening can have a profound effect on component life, reducing the number of cycles to failure by fatigue and creep life in hours by factors of 10 to 20, and this despite the fact that the cyclic stress range is well below the initial yield range in some cases. For instance, in the testing of a Bridgman notch bar with a nominal net stress at the root of 171 MPa, the Mises effective stress is only 128 MPa, well below the initial yield stress of 310 MPa. The life, however, is only 4372 cycles. From the extrapolation of the rapid cycle data, the cyclic life at this load level is predicted as about 30,000 cycles, and a theoretical prediction based upon initiation at the notch root is nearly 70,000 cycles. Similarly, the creep life predicted from the steady load effective stress at the notch is approximately 3700 hours. In view of the fact that the load reversal is rapid, so that the cyclic stress distribution is approximately elastic, the stress range through most of the notch section is considerably less than the steady creep effective stress reaching only 124 MPa at the center. This demonstrates that cyclic softening can cause serious reduction of cyclic life at even modest strain levels.

On the basis of this evidence alone, it might be concluded that there is little point in heat treating a low alloy steel to improve its initial strength, if this is to be lost later as a result of cyclic softening. Before accepting this as a general conclusion, it should be observed that a notched bar is a very severe test of stress concentration effects because the entire cross-section of the component is affected by any stress redistribution which may result from plastic deformation at the notch root. In an effort to simulate a more realistic

situation, some of the notched bar tests were performed under an R-ratio of 0, thus ensuring that only a small volume of material near the notch root experienced stress reversals. These tests show little or no overall deterioration due to softening. As shown in Table 3, the Bridgman specimen showed no significant reduction in life compared with a similar steadily loaded specimen.

d) Tensile Properties After Cyclic Loading

Following indications that the low alloy steel softened continuously during its fatigue life and that the creep strength was significantly reduced after only a limited number of fatigue cycles, a test was run to determine elevated temperature tensile properties after the material was cycled to about 10% of its failure life. The results are shown in Table 4 and these clearly indicate that the material softens considerably even during initial cyclic loading. The most drastic change is in the yield properties, though the ultimate strength is also reduced.

2.2.2 Discussion of Experimental Findings

It is concluded that the effect of cyclic softening on component behavior is extremely complex and far from being understood well enough to make full use of materials displaying this phenomenon. Clearly there are some situations in which the residual strength is little different from the same material in the annealed form, and in such cases there is no advantage in performing expensive heat treatment. A situation like this might arise, for instance, in a tube wall experiencing severe thermal gradients. On the other hand, there are many practical situations where cyclic stress reversals are confined very locally, to notches or thin surface layers in thick vessels, or where there are clearly no cyclically reversing stresses at all. It would be unjustifiably conservative, in these cases, not to utilize the improved strength gained by heat treatment. It is easy to identify the extremes of the spectrum. What remains to be done is to determine some reliable criterion for distinguishing between situations in which cyclic softening can be ignored from those in which it cannot.

There are two aspects to the problem just identified, the first relating to material behavior, and the second to component response to cyclic load.

a) Cyclic softening seems to require at least sign reversal of stress. Uniaxial creep tests in which the load was simply removed and replaced have shown no reduction in life compared with steady load tests. On the other hand, the required degree of reversal to cause softening appears to be significantly less than the initial, or even the cyclically softened, yield range as shown by the strong effect displayed by the notched tests under full load reversal. In order to investigate this point further, and to provide some theoretical backing for the simple cycle dependent yield criterion obtained empirically, some progress has been made in developing a constitutive model describing the cyclic softening effect. This work is described briefly in the next section.

b) The component design problem, which applies not only to cyclic softening but to a wide range of other design situations such as elastic follow-up and inelastic notch strains, is the need for a criterion to judge whether local strain concentrations are strain- or load-controlled. Local strain control amounts to saying that local cyclic softening will not interact with the component load carrying capacity. If conditions in highly strained regions can be determined as a property of the component and the load level only weakly dependent on material strength, then a detailed understanding of cyclic softening is not necessary to evaluate component performance. Some preliminary studies indicate that aspects of local strain behavior in components are, in fact, relatively independent of material constitutive behavior, and that it may be possible to define some classes of problems as insensitive to cyclic softening. These findings are discussed in the section on COMPONENT ANALYSIS.

2.2.3 Theoretical Modeling of Softening

The softening model described in this section is confined for the present to time independent cyclic loading.

The data were obtained from smooth specimen strain controlled fully reversed fatigue tests [2]. Two strain ranges, 0.5 percent and 1.0 percent, were used with both tests performed at a strain rate of 0.004/sec.

In principle, several unified constitutive models are capable of modeling cyclic softening behavior [8,9]. In practice, fitting the form of the constitutive equations to experimental data was found to be more complex than first appearances suggest. This was not simply a case of computational difficulty. The functional forms offered by these constitutive models were inconsistent with the type of behavior observed experimentally. For this reason the model described here is developed as an extension of an existing simple model of stable cyclic inelastic behavior, that has been used extensively and found to represent real material behavior with reasonable fidelity [10].

The model presented here assumes that the loading and unloading regions of the σ-ε hysteresis loop may be represented by a Ramberg-Osgood form [11]. Full details of the model are given in Ref. 12. For the uniaxial case

Total Strain $$\Delta\varepsilon^* = \Delta\varepsilon^*_e + \Delta\varepsilon^*_p \tag{1}$$

Elastic Strain $$\Delta\varepsilon^*_e = \frac{\Delta\sigma^*}{E} \tag{2}$$

Inelastic Strain $$\Delta\varepsilon^*_p = \left(\frac{\Delta\sigma^*}{C}\right)^{1/m} \tag{3}$$

An asterisk (*) superscript is used to indicate specific stress and strain values in individual hysteresis loops. For notation see Table 5 and Fig. 10. It should be noted that the use of a nonconventional notation for the constants in Eq. (3) above was done deliberately so as to emphasize the difference between these values and those commonly used to describe a materials cyclic σ-ε curve.

To include strain induced softening, it is assumed that C and m are functions of the cumulative plastic strain only. This is an intuitive assumption based on empirical observations of softening behavior in a number of diverse situations [5]. It appears to be the simplest assumption that is capable of capturing the essentials of softening.

This means that

$$\Delta\sigma^* = C(\Sigma\Delta\varepsilon_p) \cdot (\Delta\varepsilon_p^*)^{m(\Sigma\Delta\varepsilon_p)}. \tag{4}$$

Experimental evidence [12] shows that $C(\Sigma\Delta\varepsilon_p)$ has an n-power form,

$$C(\Sigma\Delta\varepsilon_p) = h \cdot (\Sigma\Delta\varepsilon_p)^n \tag{5}$$

where $\Sigma\Delta\varepsilon_p$ > critical strain, and $n < 0$ necessarily, to model softening behavior.

Figure 10 provides a graphical representation of these terms. As shown, the origin of the stress-strain axis is located at the beginning of the reversal. An asterisk (*) superscript is used to differentiate between relative stress-strain values (such as $\Delta\sigma^*$ and $\Delta\varepsilon_e^*$) and absolute stress-strain ranges (such as $\Delta\sigma$ and $\Delta\varepsilon_e$).

It can be shown for the material under consideration, that the relationship between stress range and strain range can be represented by

$$\Delta\sigma^* = h \cdot (\Sigma\Delta\varepsilon_p)^n \cdot (\Delta\varepsilon_p^*)^m \tag{6}$$

where h = 843 MPa, n = -0.0661, and m = 0.0905.

The above relation provides a model of the stress-strain response of a softening material subjected to a cyclic loading. This model was developed from data obtained from a fully reversed 1.0 percent strain range cyclic test. The predictive capability of this model was evaluated by comparing predictions with the experimental results of a fully reversed 0.5 percent strain range cyclic test. In predicting material response, a forward solution method was used to estimate the accumulated plastic strain at a variety of cycle numbers. This solution process involves determining, through an iterative procedure, the absolute stress and plastic strain ranges at each of the cycle numbers of interest.

Considering the limited objectives of the work reported here, the approximate constitutive relation appears to work very well indeed. As shown by Fig. 11, the cyclic stress range for a 0.5 percent strain range is predicted very closely from an equation which was derived entirely from 1.0 percent strain range data. Figure 12 shows comparisons between experimental and predicted hysteresis loops which also display good correspondence.

Since creep deformation is indistinguishable from time-independent plastic deformation in this material, even at the microstructural level, [13] the extension of the model to time-dependent conditions should be relatively straightforward. The hypothesis has yet to be tested, but future work in this direction will assume that creep and plastic deformations are additive where strain induced softening is concerned.

2.2.4 Component Analysis

This section summarizes initial attempts to explore simple methods of analysis for components composed of strain softening material. Finite element analysis of a notched bar and a cylindrical bar containing a spherical cavity has been performed using a linear strain hardening material model in which softening has been represented by a negative hardening coefficient [14]. The object is to determine the extent to which localized plastic deformation may propagate, as the result of strain induced softening, causing the component as a whole to fail by gross yielding.

The approach is an approximate one, in which the cyclic material behavior is summarized as a series of cyclic stress-strain curves, Fig. 13, and the component analyzed for the simple case of monotonic loading into the plastic range, with the assumption of negative strain hardening.

The elastic-plastic behavior of two simple component geometries, shown in Fig. 14 are examined.

The constitutive relationship used was an elastic, linear strain hardening model with the degree of hardening or softening defined by a variable strain hardening coefficient, α, which could take negative values to represent softening behavior as illustrated in Fig. 15.

The analyses are described more fully in Ref. 14.

Recently the finite element mesh has been refined to give a more accurate representation of local notch conditions. This has been used, together with cyclic stress-strain data to obtain detailed evaluations of cyclic softening in complex stress fields. The results are currently being evaluated and will be reported in the near future in a thesis to be presented by J. L. Handrock.

The only result to be discussed here is the relationship between the stress and the strain at the point of maximum strain concentration. As illustrated in Figs. 16 and 17, this relationship traces out a generalized hyperbolic locus, for a fixed load level, as the strain hardening/softening coefficient varies. In the case of a pure strain controlled situation, the locus is a vertical line at constant strain while, for load control (i.e. statically determinate), the locus is a horizontal line at constant stress, Fig. 18. Neuber's hyperbolic rule is intermediate between these extremes and is adopted in this paper as an arbitrary dividing line between local behavior which is strain or load dominated.

Results are summarized in Figs. 16 and 17. The stresses and strains refer to the mid-element Mises effective stresses and strains in the most highly strained element.

In all cases, the locus of stress versus strain with changing strain hardening index shows a clear trend which extends continuously from positive to negative values of the hardening coefficient. Not surprisingly, the Neuber rule is not correct for any of the geometries examined although it could present a first-order approximation for initial design scoping calculations. The main observation is, however, that the relaxation characteristics at a point of local inelastic deformation follows a trend which is not strongly dependent on the particular material constitutive relation and applies equally well whether the material hardens or softens as long as the inelastic strain is not too much greater than the elastic strain. To a first approximation, therefore, if a Neuber analysis is considered adequate for dealing with local inelastic deformation of a strain hardening nature, the same form of analysis should be acceptable if the material strain softens.

It can be inferred from the observations described in the previous paragraph that local deformations are largely a function of the component geometry. If so it should be possible to isolate this dependency as a parameter of the component without any reference to the detailed material behavior. So far no clear candidate for this purpose has been identified but work with simpler structures, such as three-bar structures, is being done to develop better understanding [14].

Inelastic deformations of a component can be reduced to a small number of elastic calculations to produce the peak stress-strain locus while the constitutive behavior can be considered as a virtually independent problem. Separation of essentially structural behavior from material behavior is a considerable simplification which should significantly reduce the amount of computation needed when complex constitutive relations are involved. More importantly, this separation allows predictions to be made for situations where the current knowledge of material constitutive behavior has not yet advanced to the state where it can be represented in the explicit form required for input to a full analysis - as is the case at present with strain softening.

2.3 Creep-Fatigue-Environment Effects

Uniaxial strain-controlled fatigue tests were performed at 565°C (1050°F) and a 0.50 percent fully reversed strain range under a variety of loading conditions. The entire test program is summarized in Table 6.

2.2.1 Material Response

Basic material response was the same for both smooth and prenotched specimens and in both air and vacuum environments. In all tests the material exhibited rapid cyclic softening during approximately the first twenty percent of life. Thereafter the softening rate decreased as the hysteresis loop stabilized. This response is illustrated in the stress range versus fraction of fatigue life graph of Fig. 19. The rapid decrease in stress range after about seventy percent of cyclic life is due to formation of long cracks. After this point stress decreased quickly up to failure. This overall behavior is in good agreement with other studies of bainitic 2.25Cr-1Mo [6,15,16,17].

During constant strain hold period tests, the material relaxed considerably with a corresponding gain in creep strain. Typical relaxation behavior is shown in Fig. 20. It is seen that stress relaxed in an exponential-like manner, decreasing very rapidly the first few seconds but only slowly thereafter. Relaxation rate in tension and compression were essentially identical. The amount of relaxation decreased as the material softened, throughout the duration of the test (see Fig. 21). Similar relaxation behavior of bainitic 2.25Cr-1Mo was reported by Breuer et al. [17].

2.2.2 Effect of Hold Periods

The introduction of a hold period into the hysteresis loop caused a significant reduction in fatigue life compared to the continuously cycled case (no hold period) as seen in Fig. 22. This was true regardless of the type of hold period (tensile, compressive, or combined tensile/compressive) or its duration.

In air, tensile holds were generally somewhat more damaging than compressive holds, but the combined tensile/compressive waveform was considerably more damaging than either of the previous cases. Hold periods also caused the stress range to be considerably reduced from the continuously cycled case, as shown in Figs. 19 and 22, almost immediately. In general, there was little difference in the amount of stress range reduction between the various types of hold time waveforms.

The effect of hold period duration was not marked. With only two exceptions, the six minute tensile hold test and the 0.6 minute compressive hold test, hold periods of shorter duration for a given waveform yielded higher lives. However, this trend was not strong and hold period duration had only minor influence on fatigue life. This is seen in Fig. 23, which compares stress range versus cycles for various hold time durations for the combined tensile/compressive hold waveform. Such behavior could indicate a saturation effect (i.e., after a certain point, the hold period duration has no effect) which has been proposed elsewhere [18], or perhaps more plausibly, may suggest that the hold periods were not long enough for time dependent effects to become sig-

nificant. The constant strain hold waveform and temperature, however, were such that considerable stress relaxation occurred during each hold period throughout the entire test (see Fig. 21). Of courses, this results in an increase in plastic (i.e. creep) strain and a corresponding decrease in elastic strain since the total strain remains constant. This increase in creep strain is almost certainly deleterious to fatigue resistance. Thus the most reasonable explanation for the only marginal effect of a hold period duration is the kinetics of the stress relaxation. During a constant stain hold period, stress relaxes in an exponential-like fashion, decreasing very rapidly the first few seconds but only slowly thereafter. Therefore most creep strain occurs quickly, with little difference in total creep strain for the hold period durations studied here. This behavior is illustrated in Fig. 24, a graph of percent of peak stress versus time (at half the failure life) for various tensile hold period durations. Even though hold time duration varies by an order of magnitude, there is only marginal difference in the ultimate percentage of peak stress. Similar relaxation behavior of 2.25Cr-1Mo steel has been reported elsewhere [17].

The hold period data in air is summarized in Fig. 25, which plots log time to failure versus log cycles to failures. The figure indicates the overall effect of hold periods, including the trends of the three different hold period waveforms for various hold time durations. It is seen that the symmetrical tensile/compressive hold waveform is most damaging, followed by the tensile only hold and then the compressive only hold waveforms. The relatively minor influence of hold period duration is illustrated by the nearly vertical slope of the dashed lines. Note also that the dashed lines all roughly intersect the pure fatigue datum point. All the data are quite consistent with the exception of the six minute tensile hold point (life greater than expected) and the 0.6 minute compressive hold point (life less than expected).

2.2.3 Effect of EDM Notches

In air, electro-discharge-machined (EDM) notches reduced cyclic life by an average of 22 percent compared to analogous tests of smooth specimens. The largest decrease was observed in the pure fatigue case; there was little effect on the combined tensile/compressive hold period test. Both the six minute tensile hold and six minute compressive hold tests experienced approximately a 25 percent reduction in life. EDM results in air are summarized in Fig. 26. In every case the specimen failed at one of the notch pairs.

The deleterious influence of hold periods on fatigue resistance, regardless of their location in the hysteresis loop or their duration, immediately suggests the presence of a strong creep interaction. If creep was the sole damage mechanism, however, the results of tension only hold period tests and compression only hold period tests should be similar since creep rates are equal in tension and compression. In every case, however, tensile hold tests yielded lower lives than analogous compressive hold tests. The EMD notch data offer an explanation for this behavior.

If an EDM notch is considered as a nucleated fatigue crack, these results verify that the majority of useful life is consumed by crack propagation. This is a reasonable conclusion in that the material is quite ductile and testing is in the low-cycle fatigue regime; hence substantial plastic deformation is expected and cracks should initiate fairly quickly.

Since tensile holds are more damaging than compressive holds, and the major portion of fatigue life is spent in crack growth, it follows that tensile holds promote crack propagation. This makes sense intuitively in that the crack tip is subjected to a greater stress intensity factor. Furthermore, the ingress of aggressive environment to the crack tip is facilitated while the crack is held open. Compressive holds, on the other hand, do not induce tensile stresses at the crack tip (except for possible oxide "wedging" action) and therefore do not enhance propagation rates. Compressive holds reduce life from the continuously cycled case primarily through th accumulation of creep strain. Thus both tensile and compressive hold period waveforms are

more harmful than pure fatigue due to the stress relaxation-induced creep strain, but it is the additional factor of increased crack growth rate that makes tensile holds more damaging than analogous compressive holds.

It follows logically that the combined tensile/compressive waveform, since it amasses practically twice as much creep strain, has a yet greater fatigue reduction factor than either of the above cases. Again, this is due to the exponential-like stress relaxation during the hold periods; hence two hold periods per cycle result in nearly double the creep strain as one hold period in either tension or compression despite the same overall cyclic frequency. Furthermore, the tensile hold portion of the waveform aids crack propagation.

If crack growth is indeed the controlling fatigue mechanism, one would anticipate several initiation sites, one of which grows into a crack of substantial size. Indeed, this seems to be the case as scanning electron micrographs reveal the presence of extensive secondary crack systems (see Fig. 27).

2.2.4 Effect of Vacuum

The kinetics of oxidation is extremely rapid at elevated temperature, and environmental degradation can affect the results of even very short duration tests. Of course, the influence of oxidation increases with time, and as seen in Table 6 and Fig. 25, even very brief hold periods of 0.6 minute cause time to failure to increase by sevenfold over the pure fatigue case. Naturally, for longer hold periods the gain in testing time is even more dramatic, with some tests lasting over 200 hours. At the 565°C (1050°F) test temperature, such lengthy tests permit sever oxidation. Hence the possibility was considered that environmental degradation may be the primary damage mechanism in high temperature time dependent fatigue. Therefore selected tests were conducted in a vacuum atmosphere to better ascertain the influence of oxidation on fatigue life.

Testing in a vacuum environment resulted in a significant increase in fatigue resistance for all waveforms characterized. Data for smooth specimens in both air and vacuum are compared in Fig. 28; the average

gain in life for the four different waveforms is 410 percent. As expected, the increase was most dramatic for the hold period tests due to their lengthy duration and consequent severe oxidation in air at 565°C (1050°F). In fact, in vacuum the three minute compressive hold period test had a greater life than its pure fatigue counterpart. This was true for both smooth and EDM notch specimens (see Fig. 29) and may result in part from the "welding" of the crack surfaces during the compressive hold, an effect that would be impossible in air due to formation of corrosion products in the crack.

As seen by comparing Fig. 26 and Fig. 29, EDM notches have a larger fatigue reduction factor in vacuum (41%) than they do in air (22%). This implies that a greater portion of cyclic life is spent in crack initiation (again considering the EDM notch as a nucleated fatigue crack). Alternatively, one may state that oxidation aids in crack initiation. This conclusion lends credence to other theories of premature oxide-induced fatigue crack nucleation [19,20,21] in the annealed version of this material. Another possible conclusion is that crack propagation is retarded in inert atmosphere as compared to results in air. This too is in agreement with previous investigations of ferritic 2.25Cr-1Mo steel [22,23].

The combined effects of EDM notches and vacuum are illustrated in Fig. 30. This graph plots stress range versus cycles for specimens tested in pure fatigue under four different conditions: with and without EDM notches in both air and vacuum. The two trends discussed earlier are apparent. The graph shows both the enhancement of fatigue life due to vacuum and also the more severe effect of EDM notches in the inert environment.

3. AUSTENITIC STEELS

The development of austenitic alloys for advanced fossil plant applications, specifically for superheaters and reheaters, is a new program direction. This project will look at the effects of elevated temperature monotonic and cyclic loading on the materials' elevated temperature strength. Testing will be carried out at the anticipated superheater operating temperatures of 700°C and will employ specimen geometries and loading conditions used for the studies of the low alloy steels tested in the earlier phases of this project.

It is anticipated that the initial studies of the stress-strain response of the material to a variety of loading patterns at elevated temperature will lead further work in two directions. One direction is further analysis of the time-dependent effects on the materials performance. These considerations will include the effects of thermal aging, particularly under monotonic and cyclic stress, and the effects of prior thermo-mechanical processing on the materials elevated temperature strength. The second direction is the study of crack-like defects and notches on materials behavior.

The test conditions and subsequent analysis of materials' behavior will be conducted to support design, and materials and process selection associated with tubing applications in advanced fossil superheaters and reheaters.

The Fossil Energy Materials Program is still in the process of developing advanced alloy compositions based on modifications to AISI 316 SS and Alloy 800H. This project is initially concentrating on 17-14 Cu Mo stainless steel, a commercial alloy with a composition similar to a range of the most promising 316 SS modifications. The present material is in the form of a ~20 cm diameter forging, and has been sectioned to fabricate mechanical test specimens. Optical micrographs of two longitudinal views and two transverse views, one each near the inside and outside radius are shown in Fig. 31. The difference in grain size can be noted, and precipitate banding is most noticeable in the outside radius longitudinal view.

4. CONCLUSIONS

Based on the work done so far, it is considered that strain induced softening has been well enough characterized to allow sensible design decisions to be made regarding the use or otherwise of materials which display such a phenomenon.

An earlier model of cyclic softening, suitable for design purposes, which was based on the simple concept that yield strength was a function of cumulative cycles, has been confirmed by more detailed analysis.

In developing the detailed approach, a constitutive model which includes cyclic softening has been devised. Although the model is not a unified one, it has the merits of being relatively easy to fit to material data, and has, so far, shown excellent predictive capabilities.

Damage studies have shown that, in common with other steels of similar composition, the low alloy steel which underwent the majority of testing to date shows significant environmental effects in its cyclic endurance. The effect of oxidation is to reduce lives by about a factor of three. Hold times at high temperature have similar effects. Since there is no evidence of creep damage in this material under the most extreme conditions of stress, the reason for this frequency effect is still in the realms of speculation. An hypothesis which still needs to be investigated is the possibility that the changes in the effective strain hardening index at the crack tip during creep relaxation cause a higher proportion of the crack opening to be translated into irreversible deformation and therefore crack growth. It is believed that this could be a softening related effect, causing the strainhardening index to become negative after some period of creep, leading to local material instability.

A consequence of the investigation to date is the conclusion that cyclic softening is not fundamentally a high temperature problem. In fact, its worst manifestation occurs at temperatures below the creep range. Furthermore, there is only a narrow range of component characteristics which, qualitatively, lead to problems in practice due to cyclic softening. These characteristics are low strain concentrations or stress variations, combined with a high mean stress level, and cyclic stresses comparable with the yield range over a significant proportion

of the component volume. These are not frequently found in practice, but are feasible in some practical circumstances, e.g., pipework experiencing large thermal transients, as might be found, say, in superheater and reheater tubing. Further work needs to be done to determine the boundaries of the various failure modes, including softening, and particularly to investigate the location of the creep/softening boundary.

Some work has been done to map the regime of interest in cyclic softening, using a variant of the Ashby Mechanism Map concept. So far, this work is only qualitative.

No results have been obtained for the austenitic material which is to be the subject of investigation from this point onward. From the findings of earlier investigations, however, it is apparent that the components for which the austenitics are intended fall into the category where cyclic and/or age induced strength variations can have a significant effect.

5. FUTURE WORK

Future work on this project is expected to continue along two different lines. The first relates to generic aspects of aging mechanisms and their influence on component integrity. This portion of work will follow on from previous studies and will be aimed at the development of general design rules. The second thrust, which is a new development, will be an in-depth study of the effects of service conditions on the residual strength of the austenitic steels being developed by ORNL and others.

Specific tasks envisioned are:

5.1. Wrap-up theoretical studies of softening effects in components and summarize results in the form of easily applicable design rules.

At this time, it is anticipated that the results will be in the form of load and structural categorizations determining when softening needs to be considered as a significant design case. The Ashby Mechanism Map concept is being explored for this purpose.

5.2. Creep-Fatigue-Environment effects in low alloy steels

Environment-specific aspects of this problem will not be pursued as a high priority because of the highly context dependent nature of environmental effects, and the radical change of test material will undoubtedly lead to a different set of primary concerns.

A generic question still remains regarding the possible contribution of softening to the acceleration of fatigue crack growth when hold times are present. Whether the new material hardens or softens under cyclic deformation, a limited amount of further work on the 2.25 Cr - 1 Mo steel, considered purely as a model material, is planned as a means of acquiring a better understanding of the contribution of crack tip plasticity to crack growth.

5.3. Austenitic Steels

5.3.1. Basic Characterization of Mechanical Behavior

This work will follow from the types of testing carried out in the earlier stages of the program to ascertain the materials' response to complex histories including load cycles and hold times.

5.3.2. Metallurgical Studies

A high priority will be placed on tracing the metallurgical changes resulting from both pre-service and in-service thermomechanical processes. This analysis is considered to be necessary due to the complexity of the microstructural features which provide this class of materials with their high temperature strength.

5.3.3. Surface Effects

A start will be made during this project to characterize the environment-related surface effects on accelerating the formation of fatigue cracks. It is anticipated that surface treatments, such as chromizing, may have a significant influence on service performance and the work envisioned in this project is aimed at providing a baseline against which such effects can be measured in the future.

5.3.4. Component Evaluation

Theoretical and survey investigations will be carried out to determine realistic load histories for the projected superheater and reheater geometries, and these will be used to integrate the findings of the basic materials studied into an evaluation of both volumetric and surface related damage.

REFERENCES

1. Brinkman, C.R., Report ORNL-5416, Oak Ridge National Lab., Oak Ridge, TN, 1978.

2. Kschinka, B. A. et al., "An Encapsulation Technique for Conducting Mechanical Properties Tests of Metallic Specimens in a Controlled Environment Without a Retort System", submitted to ASTM Journal of Testing and Evaluation.

3. Brinkman, C. R. et al., "Time Dependent Strain-Controlled Fatigue Behavior of Annealed 2.25Cr-1Mo Steel for Use in Nuclear Steam Generator Design", Journal of Nuclear Materials, Vol. 62, Nos. 2 and 3, Nov. 1976, pp. 181-204.

4. Ellis, J. R. et al., "Elevated Temperature Fatigue and Creep-Fatigue Properties of Annealed 2.25Cr-1Mo Steel", Structural Materials for Service at Elevated Temperature in Nuclear Power Generation, American Society of Mechanical Engineers, MPC-1, 1975, pp. 213-246.

5. Handrock, J. L., and D. L. Marriott, "Cyclic Softening Effects on Creep Resistance of Bainitic Low Alloy Steel Plain and Notched Bars," Properties of High-Strength Steels for High-Pressure Containments, ed., Nisbett, E. G., MPC-27, American Society of Mechanical Engineers, NY, 1986, pp. 93-102.

6. Pejsa, P. N., "Elevated Temperature Low-Cycle Fatigue of Two Bainitic 2.25 Cr - 1 Mo Steels," M.S. Thesis, University of Illinois at Urbana-Champaign, Illinois, 1983.

7. Swindeman, R. W., "Response of Ferritic Steels to Nonsteady Loading at Elevated Temperatures," Research on Chrome-Moly Steels, ed., Swift, R. A., MPC-21, American Society of Mechanical Engineers, NY, 1984, pp. 31-42.

8. Cescotto, S., F. Leckie, and E. Abrahamson, "Unified Constitutive Models for Creep and Plasticity of Metals at High Temperature," University of Illinois at Urbana-Champaign, Illinois, 1982.

9. Slavik, D. C., "An Experimentally Based Unified Model for Isothermal and Thermo-Mechanical Loading," M.S. Thesis, University of Illinois at Urbana-Champaign, Illinois, 1987.

10. Socie, D. F., M. R. Mitchell, and E. M. Caulfield, "Fundamentals of Modern Fatigue Analysis," Fracture Control Program Report No. 26, University of Illinois at Urbana-Champaign, Illinois, 1978.

11. Ramberg, W., and W. R. Osgood, "Description of Stress-Strain Curves by Three Parameters," NACA Technical Note No. 902, July, 1943.

12. Handrock, J. L., D. L. Marriott, and J. F. Stubbins, "Development of a Uniaxial Constitutive Model for a Strain Induced Softening Material," 5th Int. Congress on Pressure Vessels and Piping, ASME, San Diego, CA, June 28 through July 2, 1987.

13. Mehler, M. R., "The Microstructural Changes of Bainitic Two and One Fourth Percent Chromium--One Percent Molybdenum Steel During Creep," M.S. Thesis, University of Illinois at Urbana-Champaign, Illinois, 1985.

14. Marriott, D. L., K. Kloos, and J. L. Handrock, "Approximate Analysis of Components Composed of Strain Softening Material," Properties of High-Strength Steels for High-Pressure Containments, ed., Nisbett, E. G., MPC-27, American Society of Mechanical Engineers, NY, 1986, pp. 103-109.

15. Jaske, C. E., N. D. Frey, and D. A. Utah, "Low-Cycle Fatigue of Heat-Treated 1Cr-1Mo-0.25V and 2.25Cr-1Mo Steels and Annealed Type 304 Stainless Steel at High Temperatures", Applications of Materials for Pressure Vessels and Piping, ASME MPC-10, 1979, pp. 175-209.

16. Swindeman, R. W., and J. P. Strizak, "Response of Bainitic 2.25Cr-1Mo Steel to Creep-Fatigue Loadings at 482°C", Report ORNL/TM-8372, Oak Ridge National Lab., Oak Ridge, TN, Nov. 1982.

17. Breuer, H. J. et al., "Mechanical Properties and Low Cycle Fatigue Behavior of Heat Treated Nb-Stabilized and Unstabilized 2.25Cr-1Mo Steel", Ferritic Alloys for Use in Nuclear Energy Technologies, The Metallurgical Society of AIME, 1984, pp. 451-9.

18. Carden, A. E. et al., "Time Dependent Fatigue of Structural Alloys - A General Assessment", Report ORNL-5073, Oak Ridge National Lab., Oak Ridge, TN, 1975.

19. Teranishi, H. and A. J. McEvily, "The Effect of Oxidation on Hold Time Behavior of 2.25Cr-1Mo Steel", Metallurgical Transactions, Vol. 10A, 1979, pp. 1806-08.

20. Challenger, K. D., A. K. Miller and C. R. Brinkman, "An Explanation for the Effects of Hold Periods on the Elevated Temperature Fatigue Behavior of 2.25Cr-1Mo Steel", Journal of Engineering Materials and Technology, Vol. 103, No. 1, Jan. 1981, pp. 7-14.

21. Challenger, K. D., A. K. Miller and R. L. Langdon, "Elevated Temperature Fatigue with Hold Times in a Low Alloy Steel: A Predictive Correlation", Journal of Materials for Energy Systems, Vol. 3, No. 1, June 1981, pp. 51-61.

22. Corwin, W. R. and C. R. Brinkman, "Effects of Steam and Helium Environments on the Elevated Temperature Subcritical Crack Growth of 2.25Cr-1Mo Steel", Proceedings of the Second International Conference on Mechanical Behavior of Materials, Federation of Materials Sciences, Boston, 1976, pp. 1498-502.

23. Corwin, W. R. et al., "Fatigue Crack Propagation in 2.25Cr-1Mo Steel", Report ORNL-5355, Oak Ridge National Lab., Oak Ridge, TN, Feb. 1978.

Table 1 Chemical composition of low alloy steel used in investigation

Component	%
C	0.13
Mn	0.53
P	0.003
S	0.003
Cu	0.16
Is	0.25
Ni	0.15
Cr	2.33
Mo	0.96
Sn	0.001
Al	0.011
V	0.01
As	0.002
Sb	0.0005
Fe	Remainder

Table 2 :- Tensile Properties of Kawasaki 2.25Cr-1Mo Steel

strain rate = 0.004 per second

		25°C	565°C
Elastic Modulus (GPa)		208	159
0.2% Yield Strength (MPa)	474	348	
Ultimate Strength (MPa)	590	380	
True Fracture Stress (MPa)	1280	838	
corrected to (MPa)*	1090	699	
True Fracture Ductility	1.53	1.94	
% Reduction of Area	78.4	85.6	
True Strain @ Ultimate Load		.076	.019
Strain Hardening Exponent	0.11	0.06	
Strength Coefficient (MPa)	855	510	

*Corrected for necking with Bridgman's Correction Factor

Table 3 Low frequency creep-fatigue test results on smooth and notched bars (tests conducted on Arc weld deadweight creep machines)

Specimen Type	σ_{net} Stress MPa	σ_{eff} Stress MPa	Cycles to Failure N_f	Time to Failure Hours	Hold Time Min	R Ratio
S	152	152		1581		1
S	172	172		476		1
B	226	169		665		1
B	226	169	6130	613	5	0
V	232	166		594		1
V	232	166	2250	225	5	0

S = Smooth specimen, B = Bridgman specimen, V = Vee-notch specimen.

Table 4 Tensile Properties of the Kawasaki 2.25Cr-1Mo Steel at 565°C in the As-Received Condition and Cycled to 10% of Failure at at a 0.5% Total Strain Range

Property	As-Received	After Cycling*
0.2% YS (MPa)	348	271
UTS (MPa)	380	352
RA (%)	85.6	85.7

*N = 320 cycles

Table 5 Nomenclature for cyclic softening constitutive model

C	Hysteresis loop strength coefficient
C_o	Cutoff value of C for small values of accumulated plastic strain (1068 MPa)
E	Young's modulus (159 GPa)
h	Strength coefficient material constant (843 MPa)
log	Common logarithm (base 10)
m	Hysteresis loop strain hardening exponent (0.0905)
n	Strength exponent material constant (-0.0661)
N	Specific cycle number
$\Delta\varepsilon$	Absolute total strain range
$\Delta\varepsilon^*$	Relative total strain range
$\Delta\varepsilon_e$	Absolute elastic strain range
$\Delta\varepsilon_e^*$	Relative elastic strain range
$\Delta\varepsilon_p$	Absolute plastic strain range
$\Delta\varepsilon_p^*$	Relative plastic strain range
$\Delta\sigma$	Absolute stress range
$\Delta\sigma^*$	Relative stress range
$\Sigma\Delta\varepsilon_p$	Accumulated plastic strain
$\Sigma(\lvert\Delta\varepsilon_{eff}\rvert)$	Accumulated Mises plastic strain

Table 6: Results of Fatigue Tests at 565°C and 0.50% Strain Range

	Specimen	Environment	Smooth or EDM	Hold Period (min.)	At Half the Failure Life: Stress Range (MPa)	Stress Amplitudes (MPa): Tensile Peak	Tensile Relaxed	Compressive Peak	Compressive Relaxed	Cycles to Failure	Time to Failure (hr.)
1	6B	Air	S	0	472	238	-	234	-	3783	2.6
2	DS-1	Air	S	6 T	406	190	132	216	-	2000	201
3	DS-4	Air	S	6 C	413	218	-	195	133	2050	206
4	A3A	Air	S	6 T+C	411	202	134	209	138	895	180
5	DS-2A	Air	S	3 T	431	201	145	230	-	1465	74
6	DS-11	Air	S	3 C	409	216	-	193	142	2245	114
7	DS-10	Air	S	3 T+C	402	201	138	201	138	905	91
8	A10A	Air	S	1.5 T	438	207	157	231	-	1648	42
9	DS-14	Air	S	1.5 C	402	209	-	193	148	2340	60
10	A7	Air	S	1.5 T+C	433	213	156	220	162	1042	53
11	DS-5F	Air	S	.75 T+C	436	218	167	218	165	1278	33
12	DS-BR2	Air	S	0.6 T	432	206	158	226	-	1662	18
13	DS-ER1	Air	S	0.6 C	435	226	-	209	160	1821	19
14	DS-16	Air	EDM	0	452	226	-	226	-	2664	1.9
15	DS-5	Air	EDM	6 T	419	197	139	222	-	1536	155
16	DS-17	Air	EDM	6 C	413	220	-	193	136	1550	156
17	DS-A	Air	EDM	3 T+C	419	213	148	206	141	803	81
18	DS-1A	Vac	S	0	450	227	-	223	-	9750	6.8
19	DS-E	Vac	S	3 T	419	196	150	223	-	5447	276
20	DS-6F	Vac	S	3 C	410	224	-	186	139	11903	603
21	DS-BR9	Vac	S	1.5 T+C	382	192	144	190	138	5001	254
22	DS-D	Vac	EDM	0	464	234	-	230	-	5276	3.7
23	DS-1F	Vac	EDM	3 T	406	189	146	217	-	3789	192
24	DS-2F*	Vac	EDM	3 C	410	215	-	195	128	5550	293
25	DS-BR4	Vac	EDM	1.5 T+C	395	198	157	197	144	3275	166

LIST OF FIGURES

Fig. 1 Standard uniform section and notched bar specimen configurations.

Fig. 2 Double shoulder specimen geometry for encapsulated testing (all dimensions are in mm).

Fig. 3 Double shoulder fatigue specimen before (left) and after (right) encapsulation for vacuum testing.

Fig. 4 Schematic of electrodischarge machined (EDM) notch specimen.

Fig. 5 Schematic of waveforms used in fatigue experiments. Strain rates used during the ramp portions were 0.004 per second, strain limits were $\pm$0.25%.

Fig. 6 Maximum and minimum stress versus number of cycles for a variety of cyclic conditions.

Fig. 7 Constant strain rate test results.

Fig. 8 Smooth and notched specimen creep tests with interspersed load reversals test data superimposed on cyclic softening curves.

Fig. 9 Theoretical versus experimental frequency dependence of cyclic strength. Experimental data point (square) consists of a Bridgman specimen creep test with superimposed load reversal every hour. Result is plotted using effective stress.

Fig. 10 Definition of stress and strain ranges for a typical hysteresis loop.

Fig. 11 Experimental and predicted results of stress range versus number of cycles for a 0.5% strain range cyclic test.

Fig. 12 Experimental versus predicted hysteresis loops at cycle number 2500 for a 0.5% strain range cycle test.

Fig. 13 Cyclic stress-strain curves.

Fig. 14 Geometries of notched bar and bar with spherical cavity.

Fig. 15 Schematic representation of the constitutive relation (α is the strain hardening coefficient nondimensionalized with respect to Young's modulus, E).

Fig. 16 C-notch peak stress versus peak strain relationship for most highly strained element.

Fig. 17 Cavity in cylinder bar: peak stress versus peak strain for most highly strained element.

Fig. 18 Schematic representation of redistribution behavior at point of peak stress.

Fig. 19 Stress range versus percent of cyclic life for EDM specimens tested in air. Note the immediate softening response and also the decrease in stress range due to the hold period waveforms.

Fig. 20 Typical relaxation behavior during constant strain hold period at half the failure life. Differences between the relaxation rates in tension and compression were negligible.

Fig. 21 Peak and relaxed stress versus percent of cyclic life showing the amount of stress relaxation throughout an entire test.

Fig. 22 Stress range versus cycles for smooth specimens tested in air indicating the deleterious effect of hold periods on fatigue resistance.

Fig. 23 Stress range versus fatigue cycles for combined tensile/compressive waveforms illustrating only minor effects of hold period duration on fatigue life.

Fig. 24 Percent of peak stress versus time at half the failure life for tensile hold period waveforms with hold times ranging from 0.6 to 6 min. Note the similarity in the amount of stress relaxation in each case despite the wide variance in the hold period duration.

Fig. 25 Iso-strain to failure versus cycles to failure diagram showing the overall effects of hold periods.

Fig. 26 Comparison of fatigue life data in air for smooth and EDM notch specimens. Average reduction in life due to EDM notches for the above waveform is 22%.

Fig. 27 Scanning electro micrograph (100X) of a typical fatigue specimen surface clearly indicating the presence of secondary crack system. The arrows indicate the loading direction.

Fig. 28 Comparison of fatigue life data for smooth specimens tested in both air and vacuum. The average increase in life due to vacuum for this waveform is 410%.

Fig. 29 Comparison of cyclic life data in vacuum for both smooth and EDM notch specimens.

Fig. 30 Stress range as a function of cycles for pure fatigue waveforms showing the effects of smooth versus EDM notch specimen geometry and air versus vacuum.

Fig. 31 Optical micrographs of the 17-14 CuMo steel forging (a) forging center, longitudinal view; (b) forging outer radius, longitudinal view; (c) forging center, transverse view; (d) forging outer radius, transverse view.

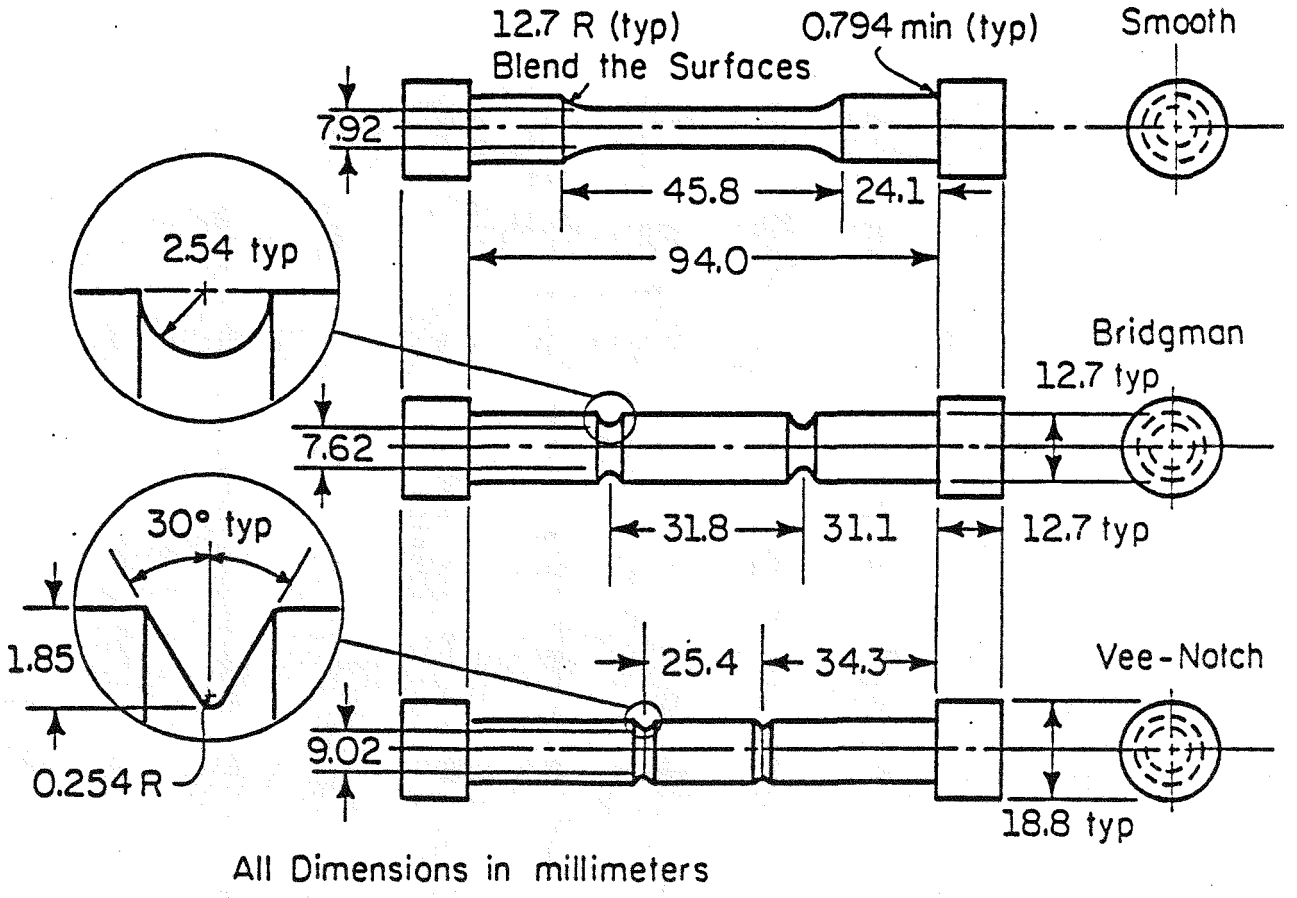

Fig. 1 Standard uniform section and notched bar specimen configurations.

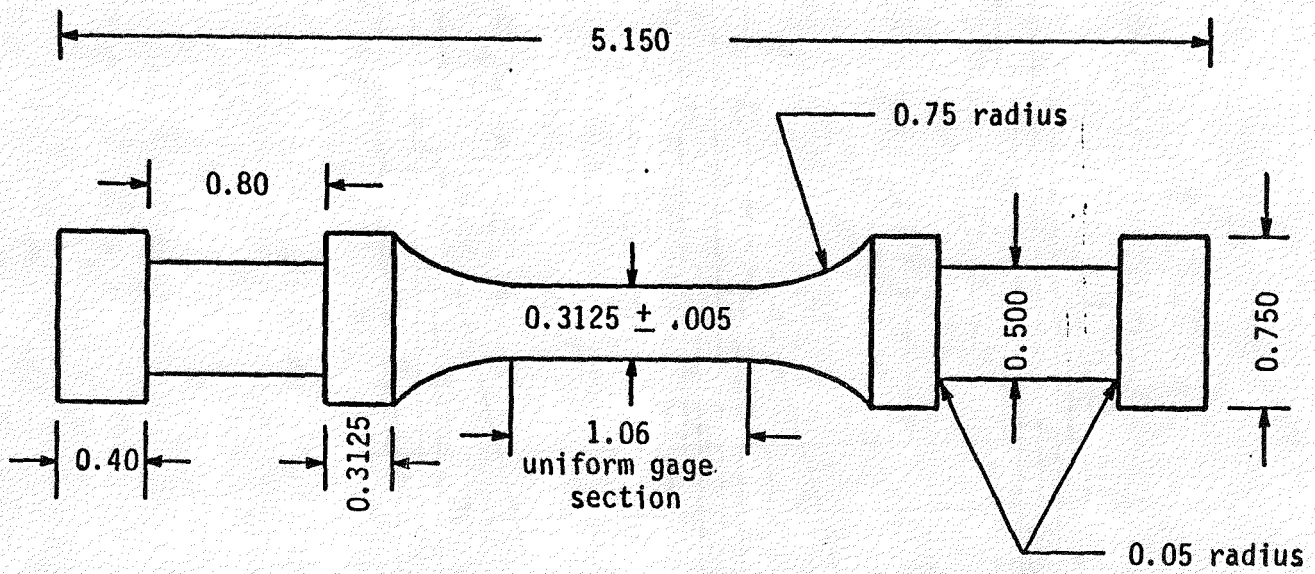

Fig. 2 Double shoulder specimen geometry for encapsulated testing. (All dimensions are in mm.)

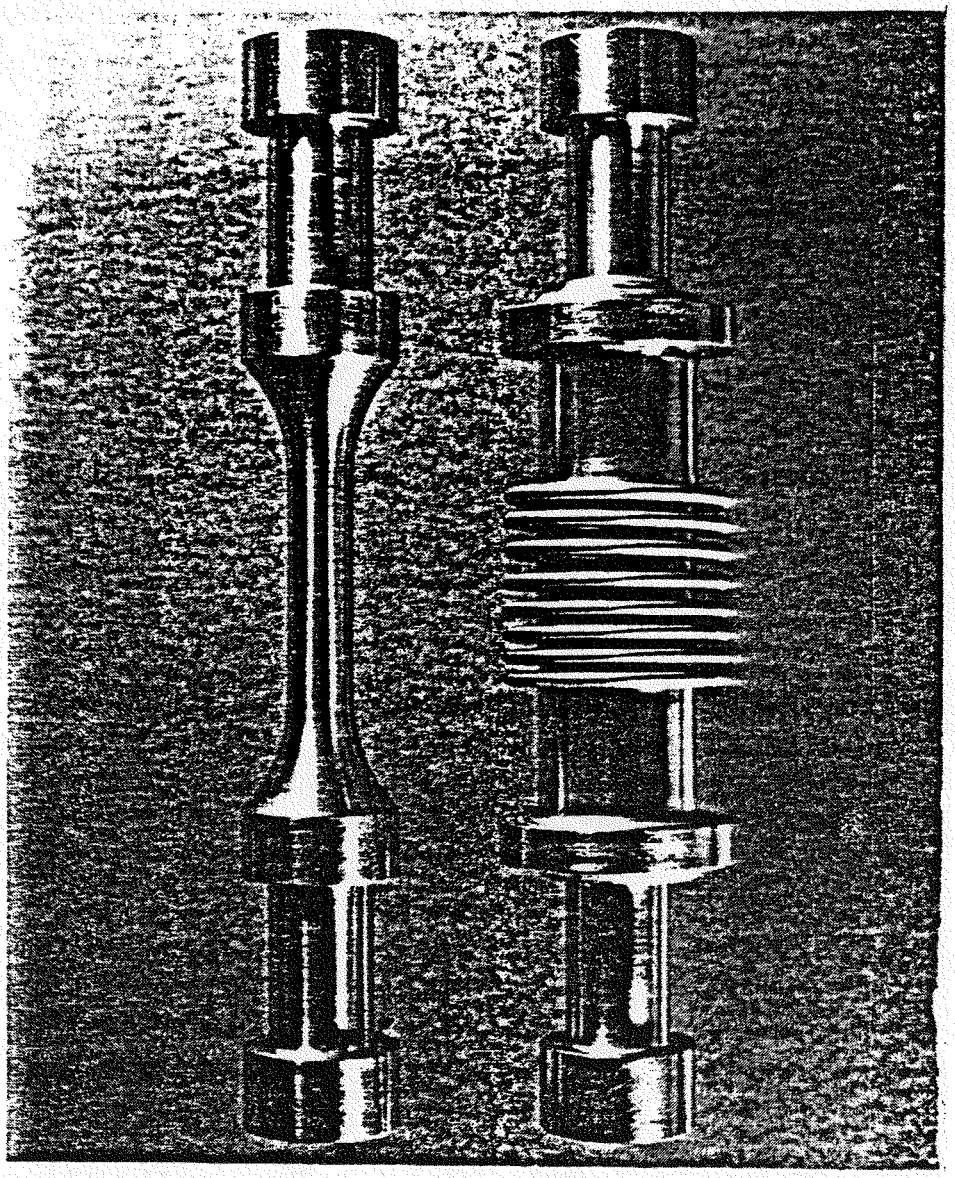

Fig. 3 Double shoulder fatigue specimen before (left) and after (right) encapsulation for vacuum testing.

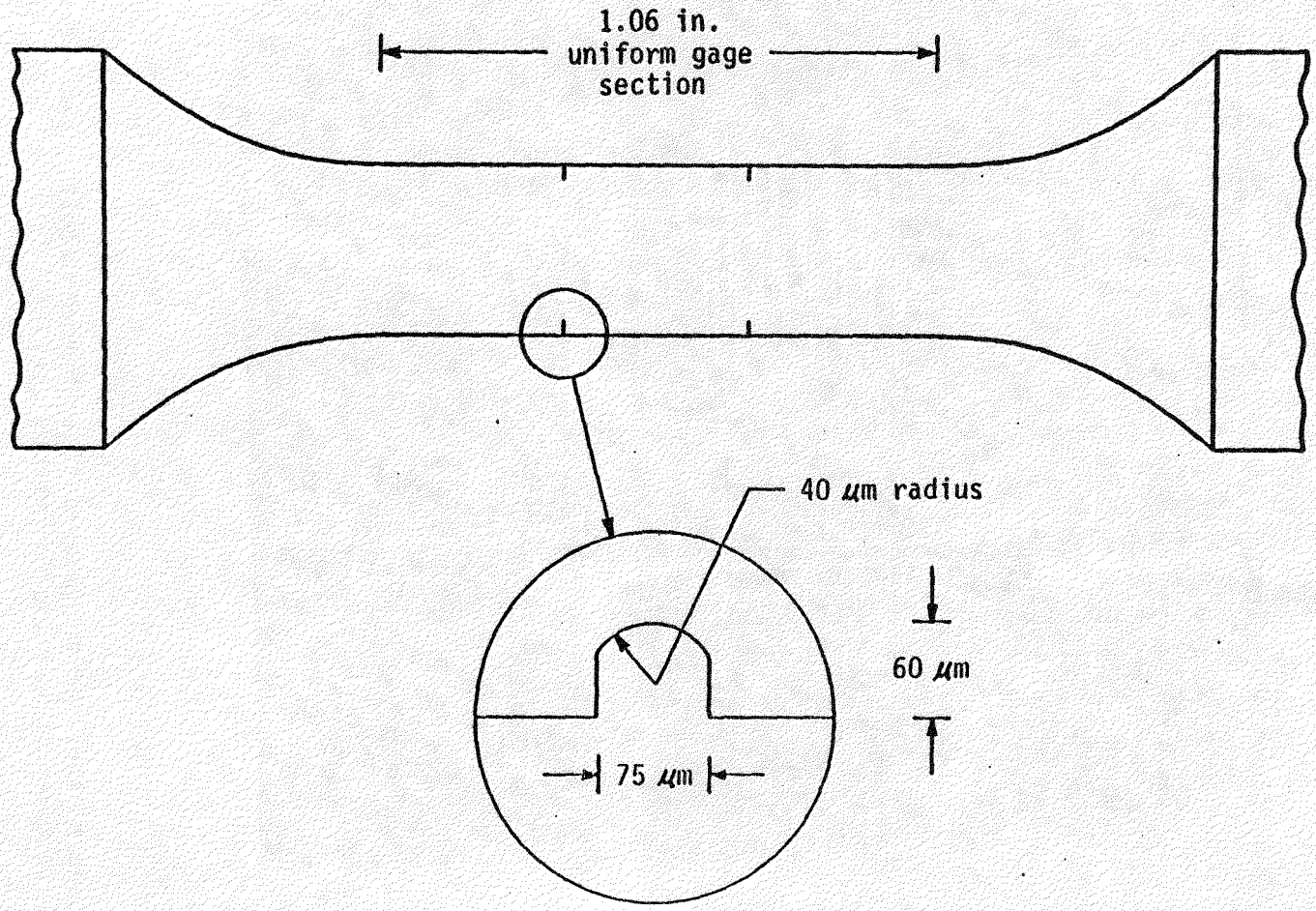

Fig. 4 Schematic of electro-discharge machined (EDM) notch specimen.

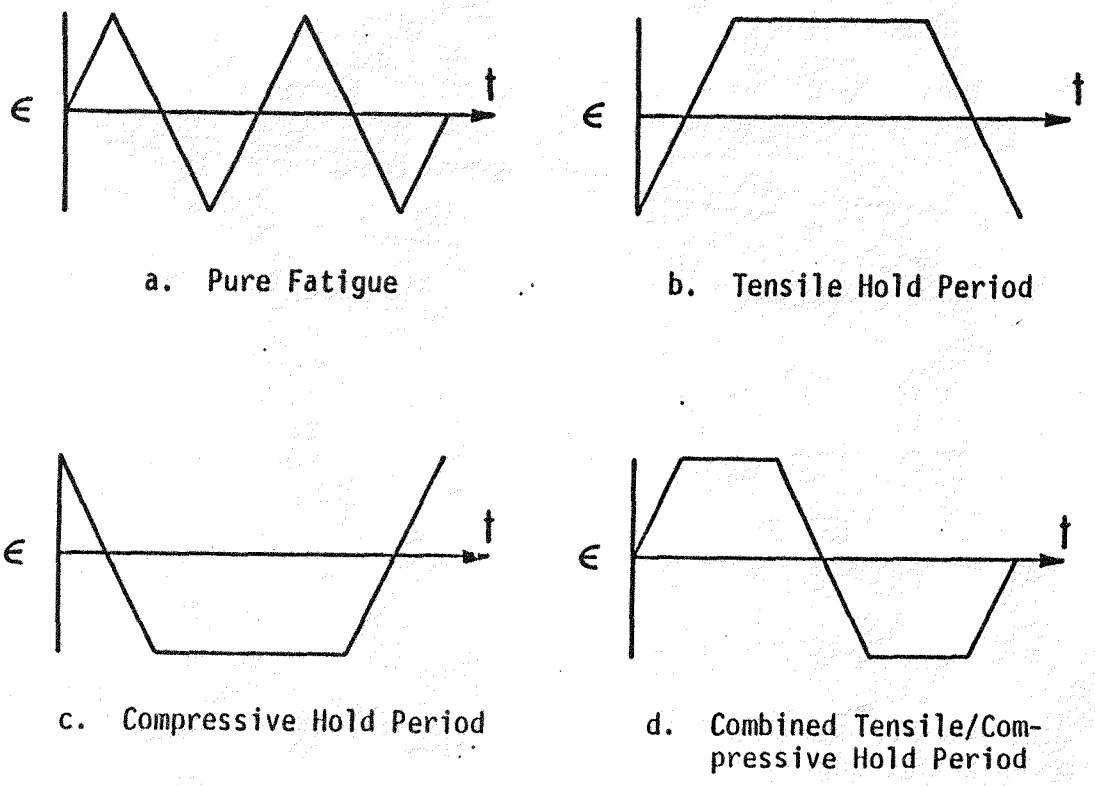

Fig. 5 Schematic of waveforms used in fatigue experiments. Strain rates used during the ramp portions were 0.004 per second. Strain limits were $\pm$0.25%.

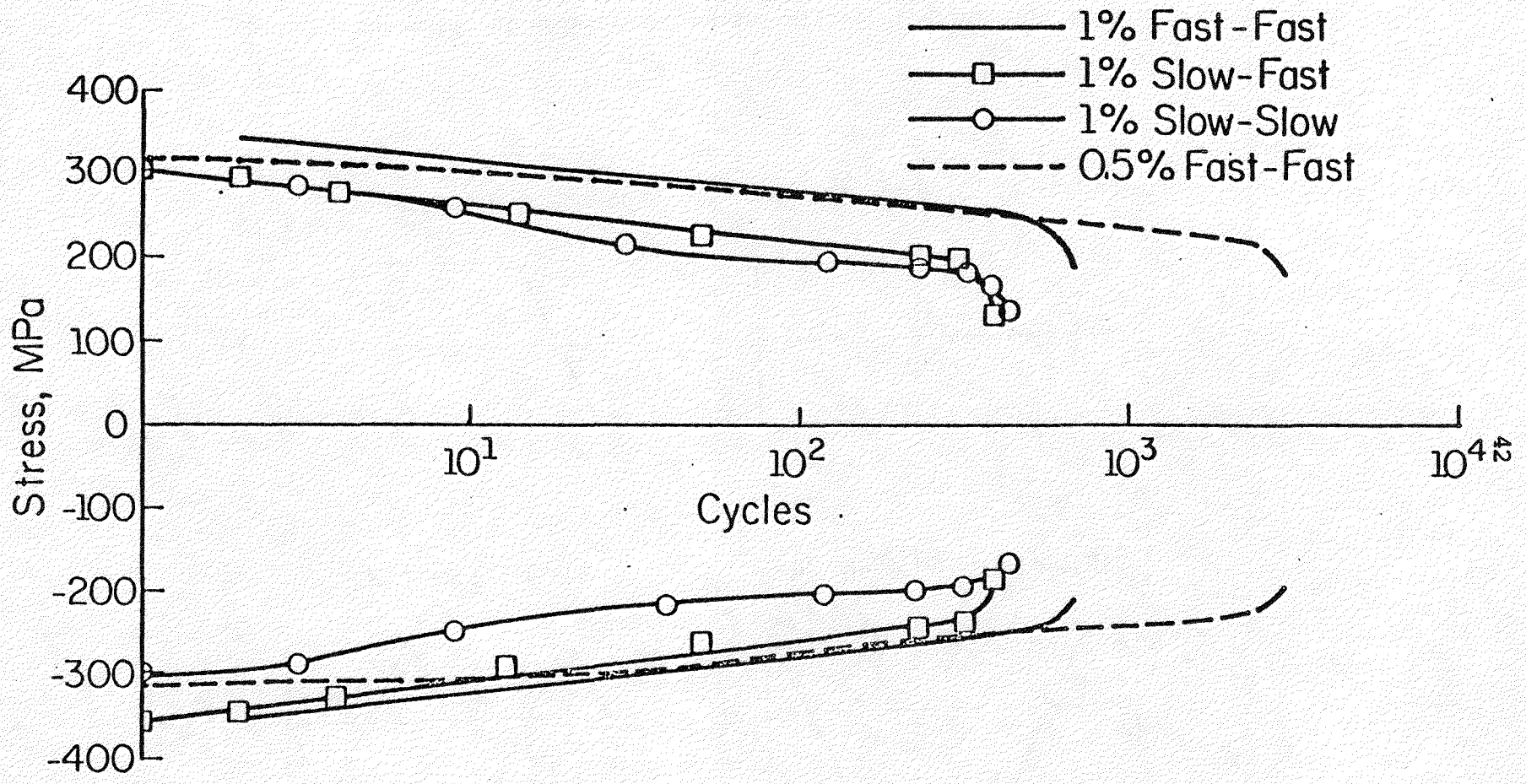

Fig. 6 Maximum and minimum stress versus number of cycles for a variety of cyclic conditions.

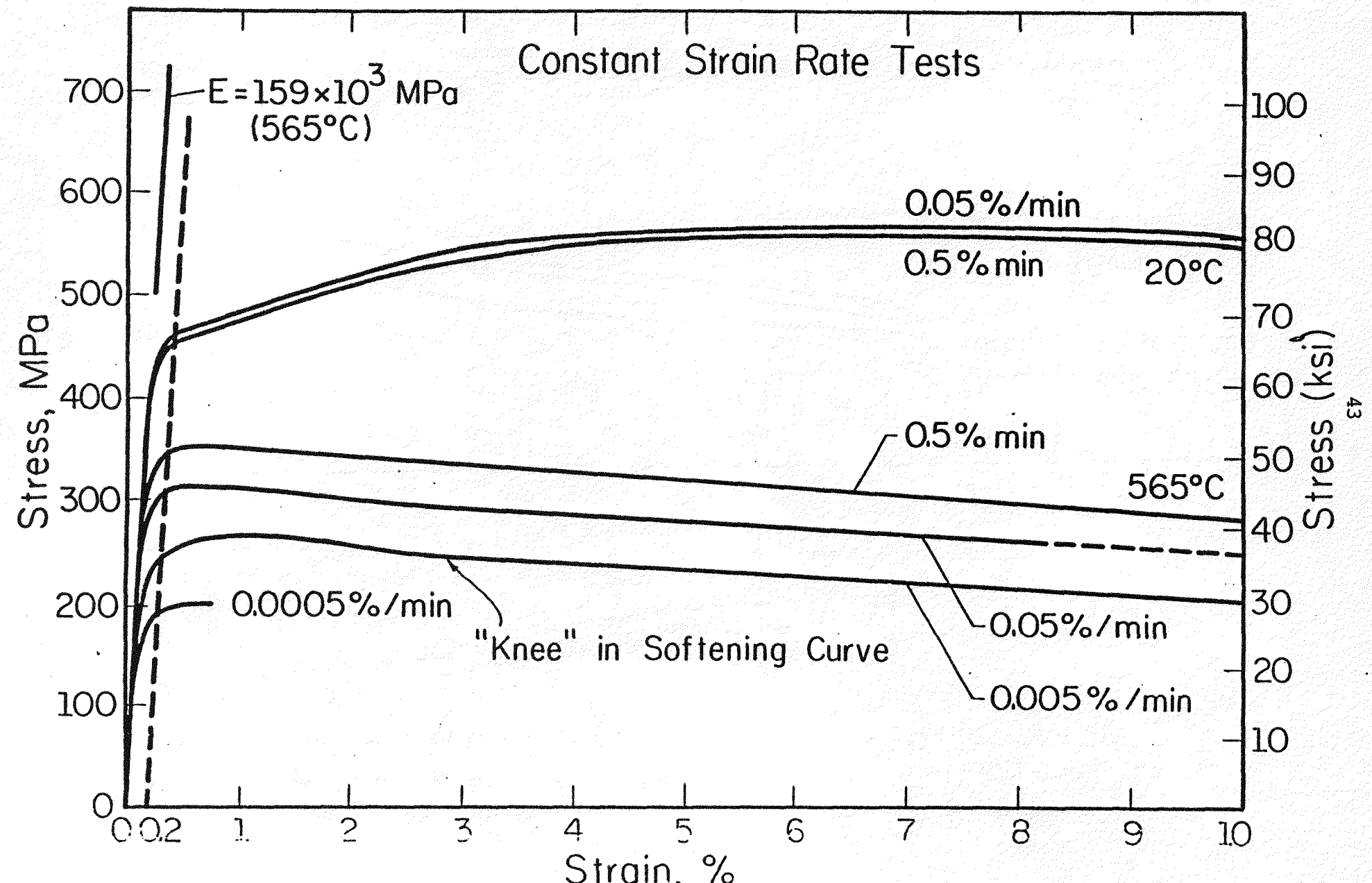

Fig. 7 Constant strain rate test results.

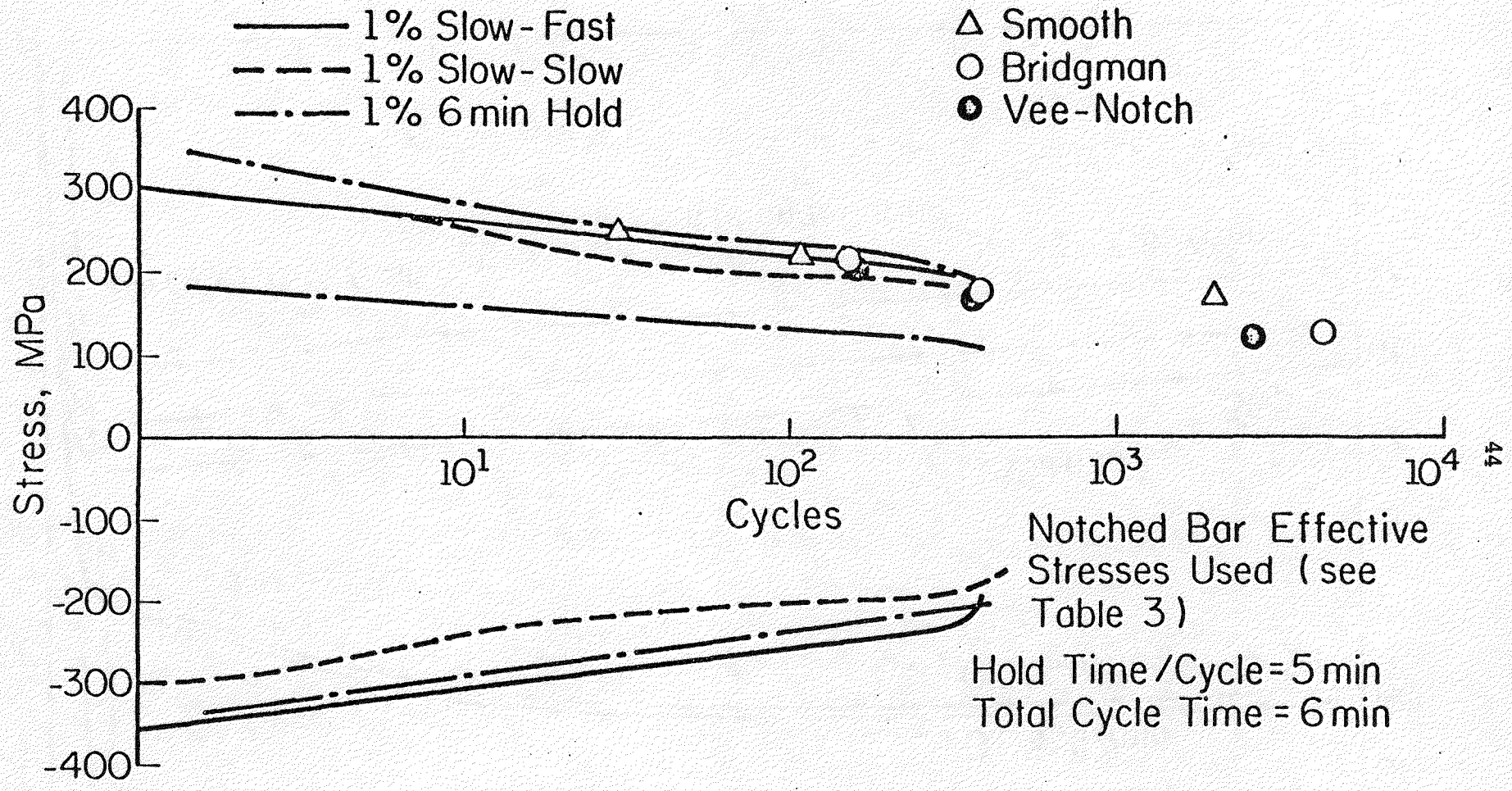

Fig. 8 Smooth and notched specimen creep tests with interspersed load reversals data superimposed on cyclic softening curves.

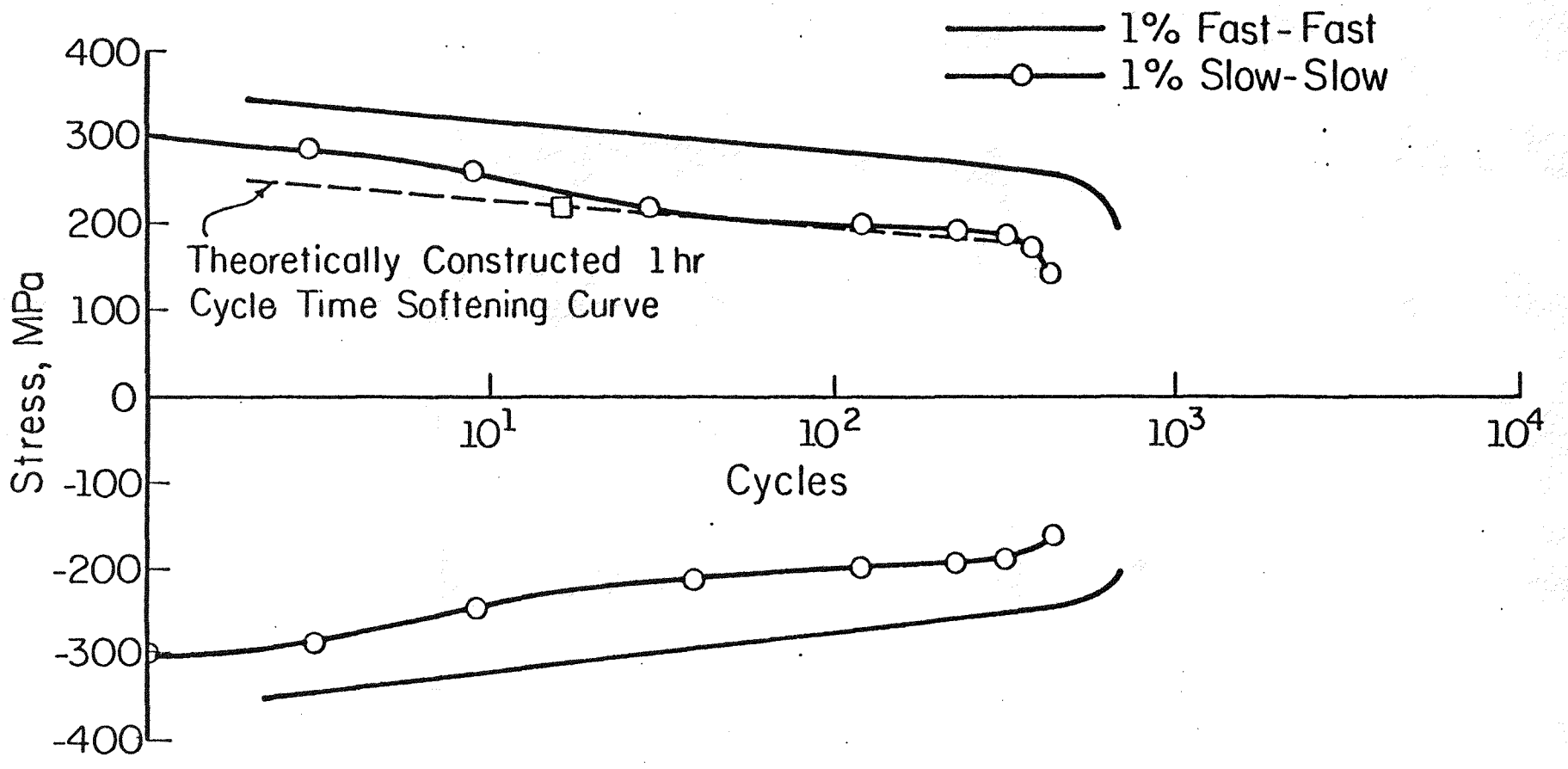

Fig. 9 Theoretical versus experimental frequency dependence of cyclic strength. Experimental data point (square) consists of a Bridgman specimen creep test with superimposed load reversal every hour. Result is plotted using effective stress.

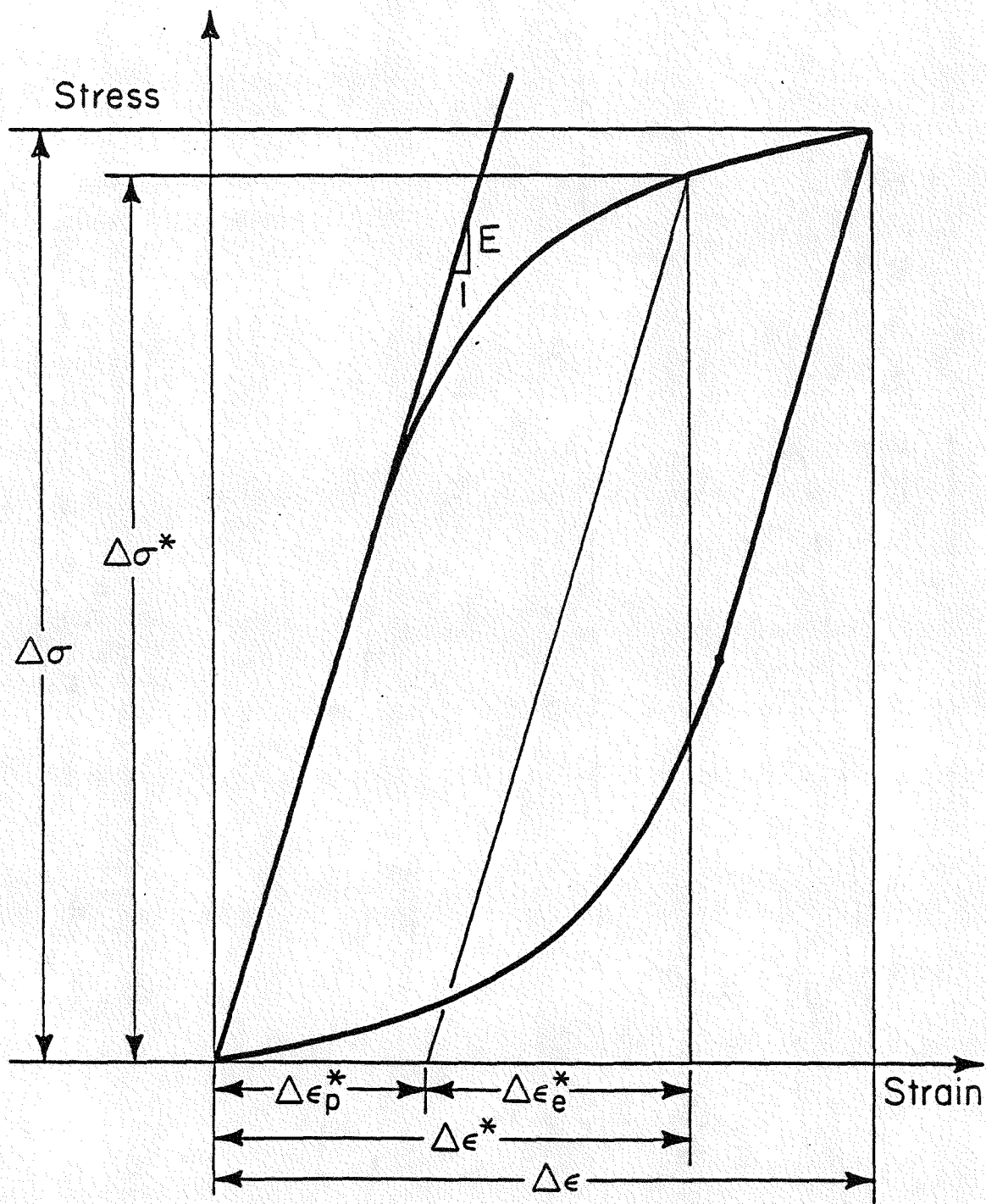

Fig. 10 Definition of stress and strain ranges for a typical hysteresis loop.

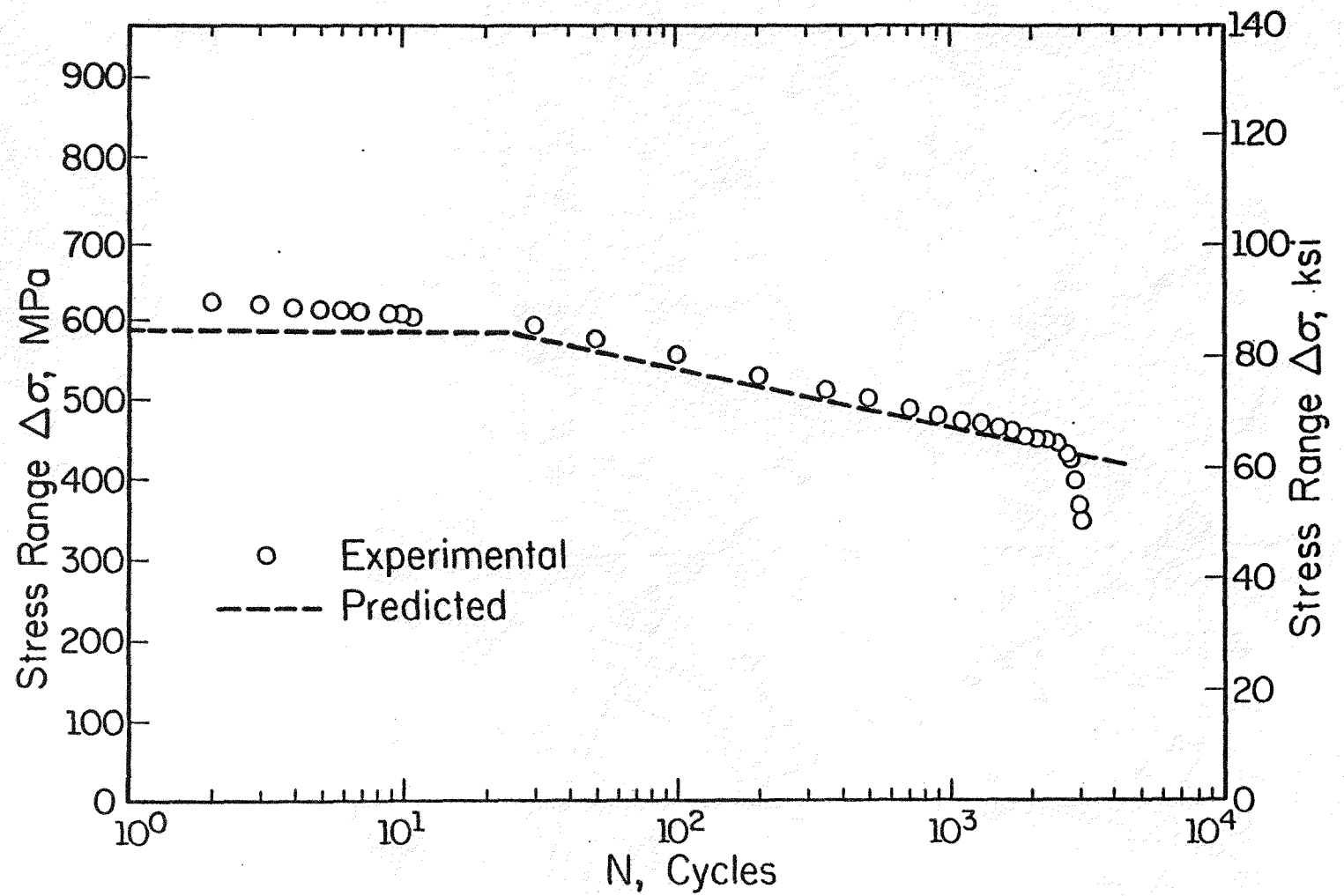

Fig. 11 Experimental and predicted results of stress range versus number of cycles for a 0.5% strain range cyclic test.

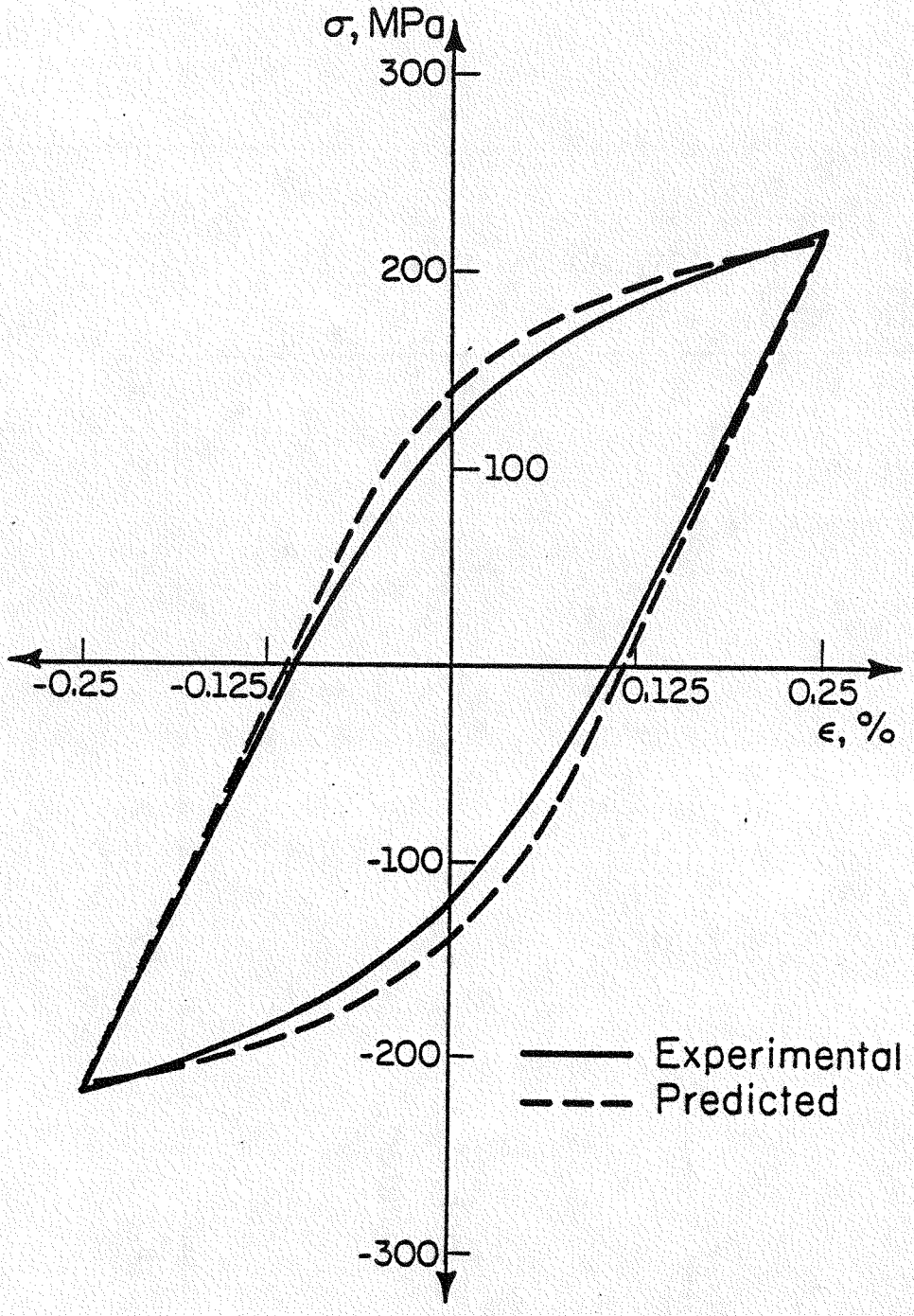

Fig. 12 Experimental versus predicted hysteresis loops at cycle number 2500 for a 0.5% strain range cyclic test.

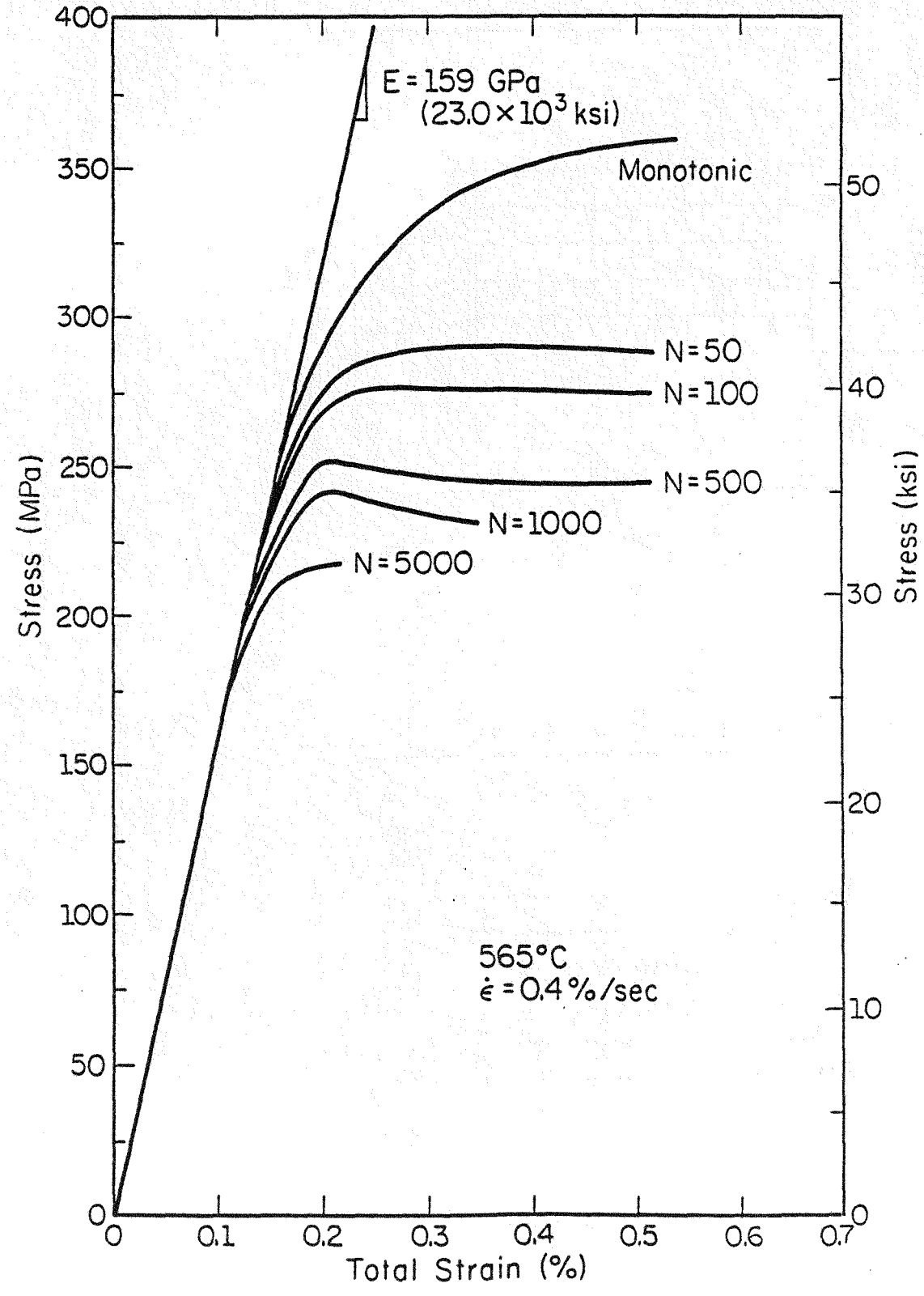

Fig. 13 Cyclic stress-strain curves.

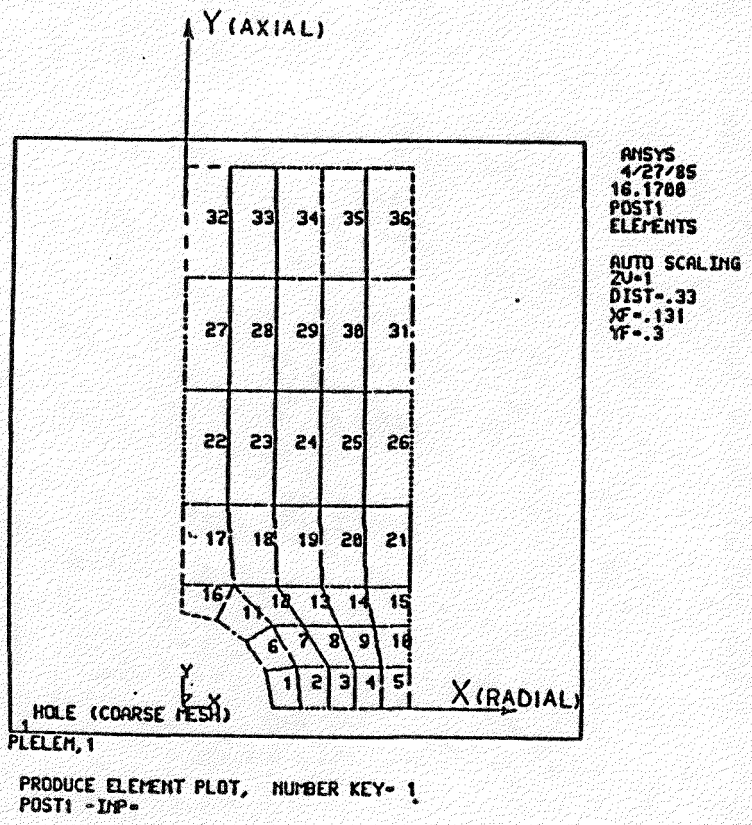

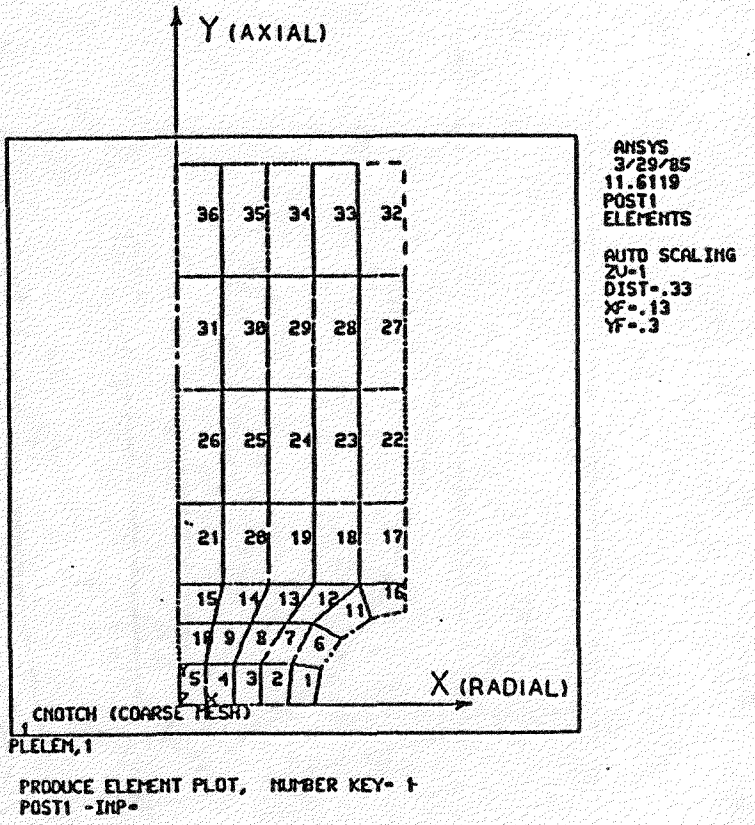

Fig. 14 Geometries of notched bar and bar with spherical cavity.

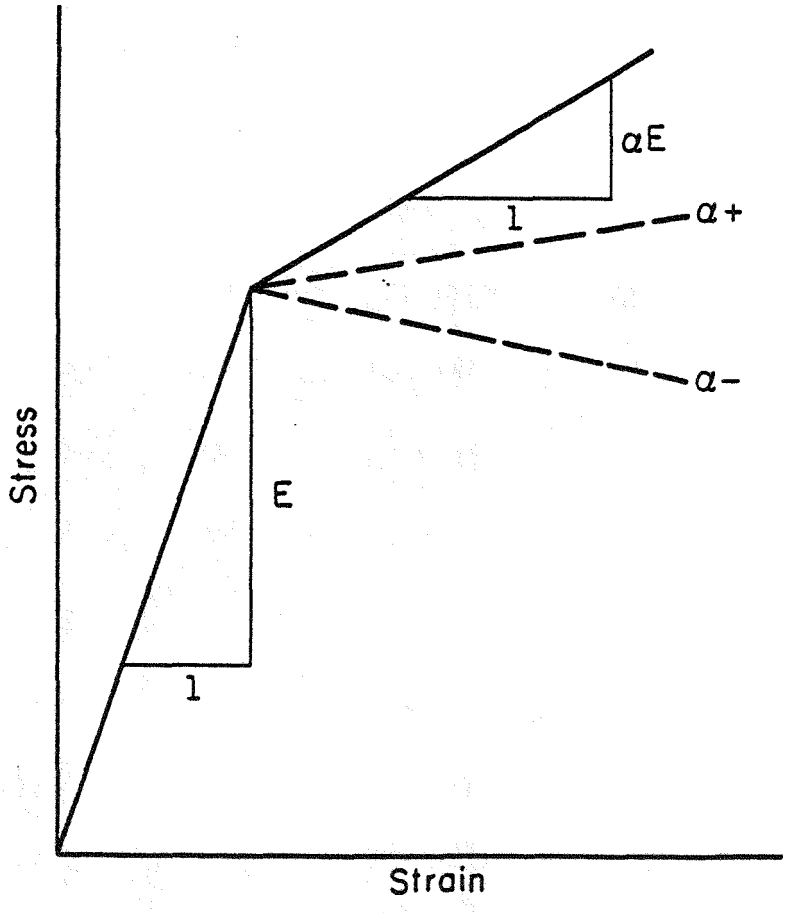

Fig. 15 Schematic representation of the constitutive relation (α is the strain hardening coefficient nondimensionalized with respect to the Young's modulus, E).

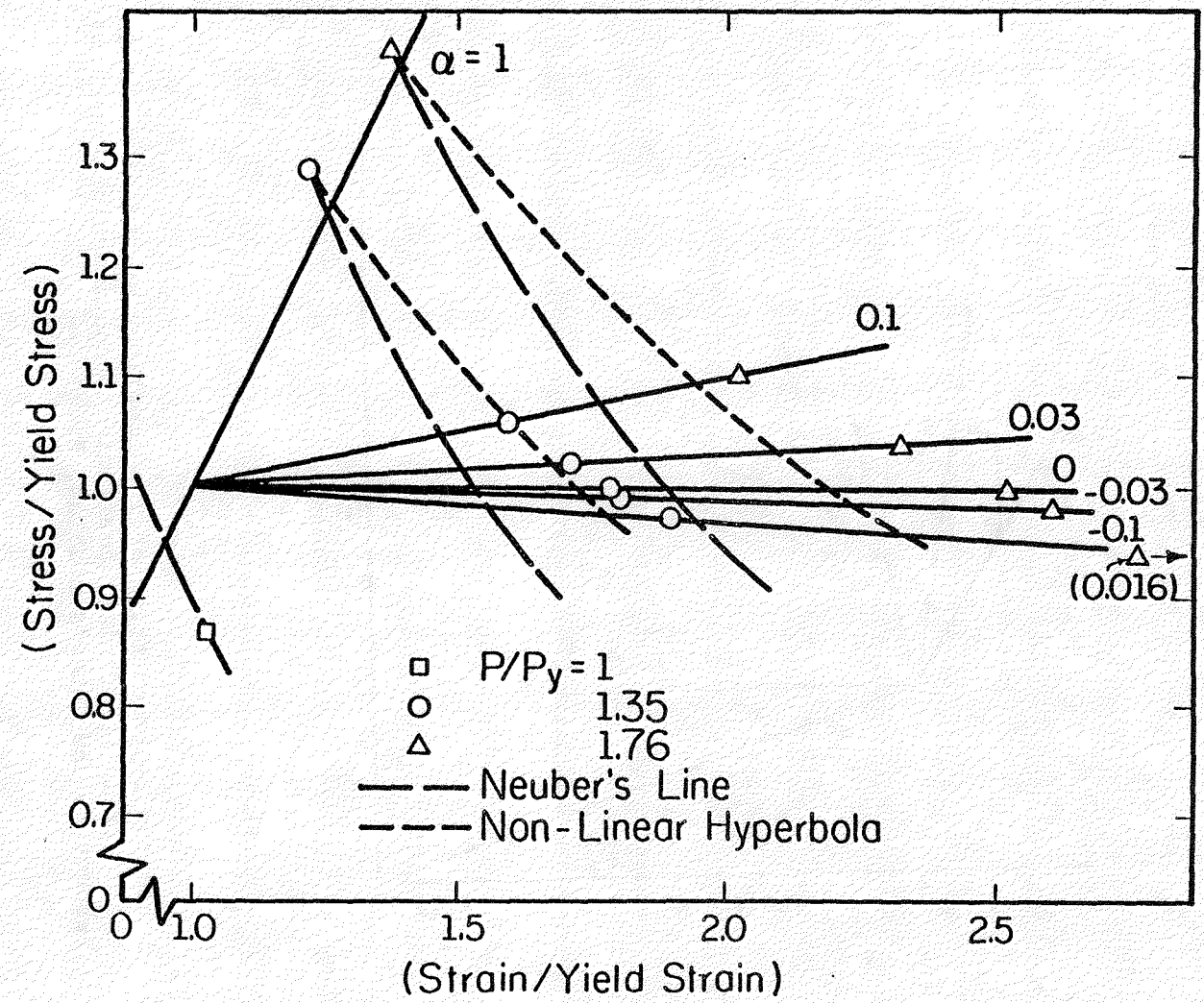

Fig. 16 C-notch peak stress versus peak strain relationship for the most highly strained element.

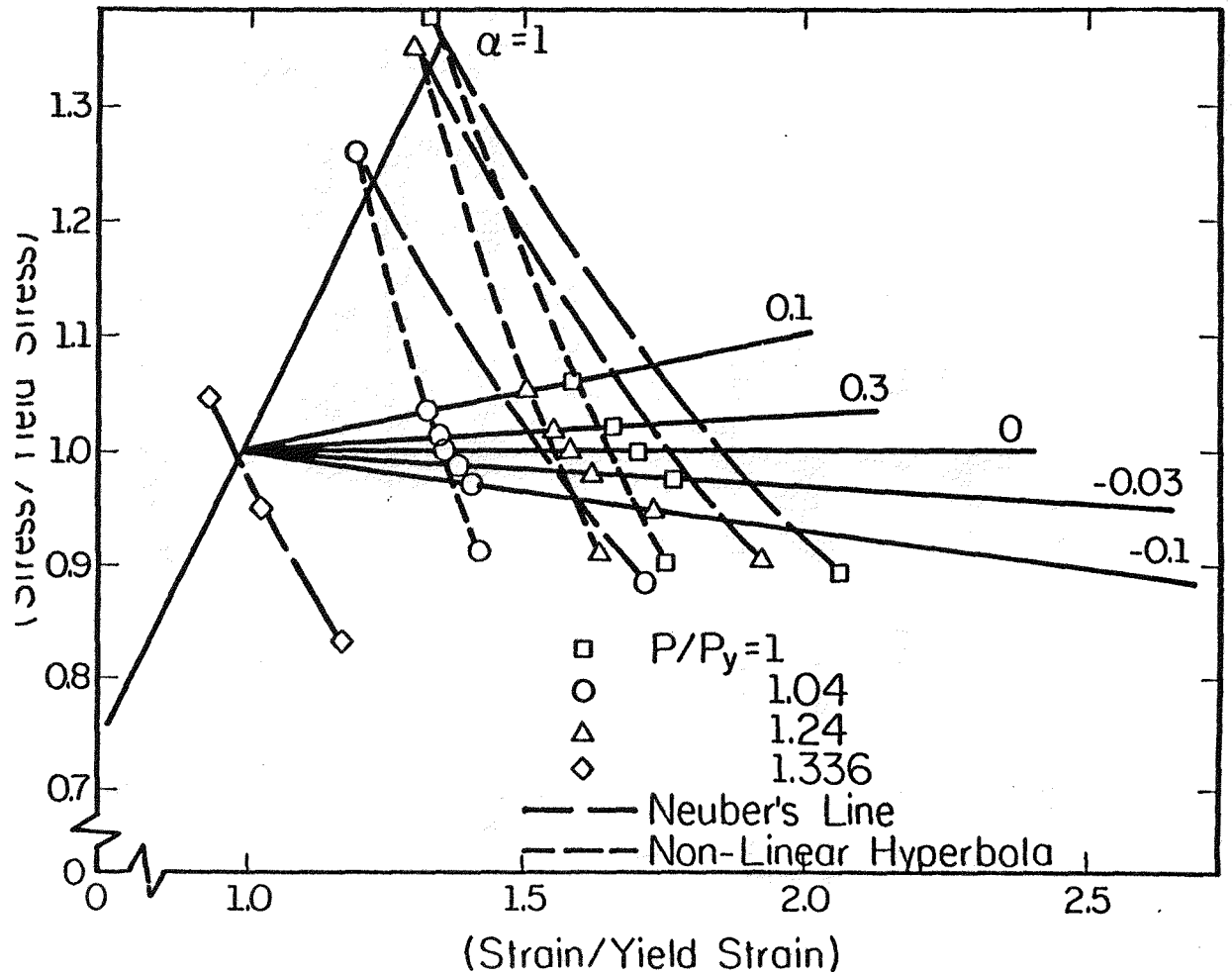

Fig. 17 Cavity in cylinder bar: peak stress versus peak strain for the most highly strained element.

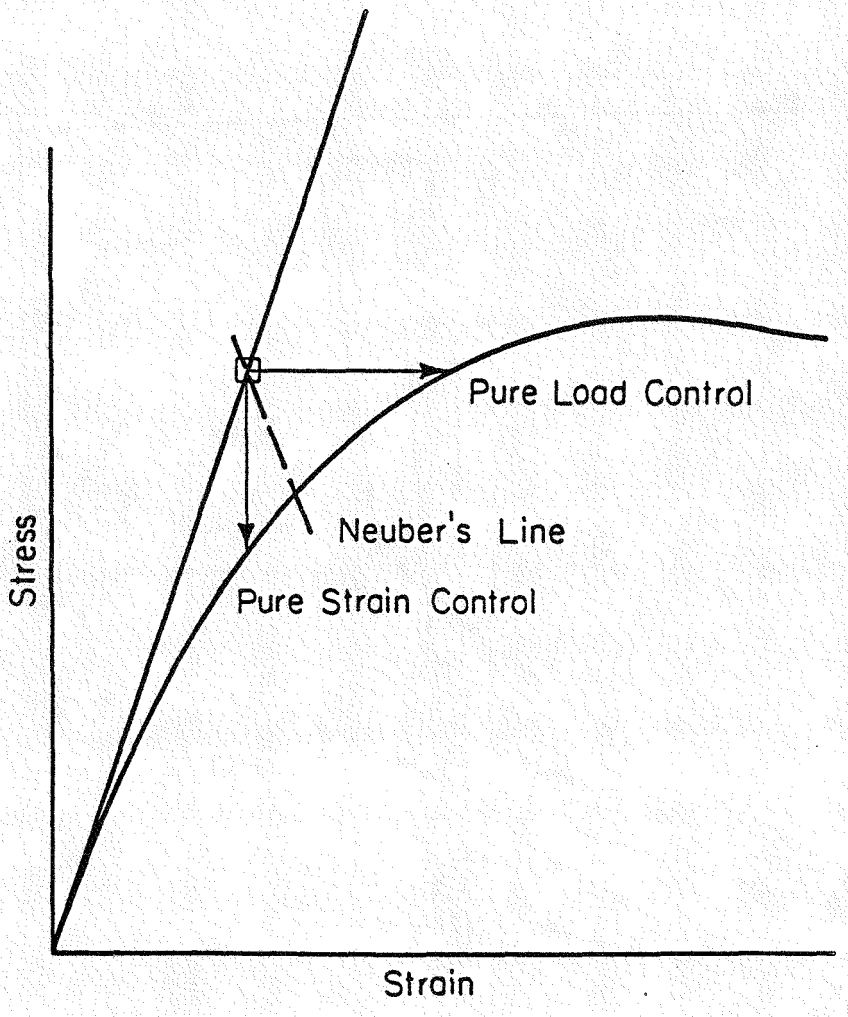

Fig. 18 Schematic representation of redistribution behavior at the point of peak stress.

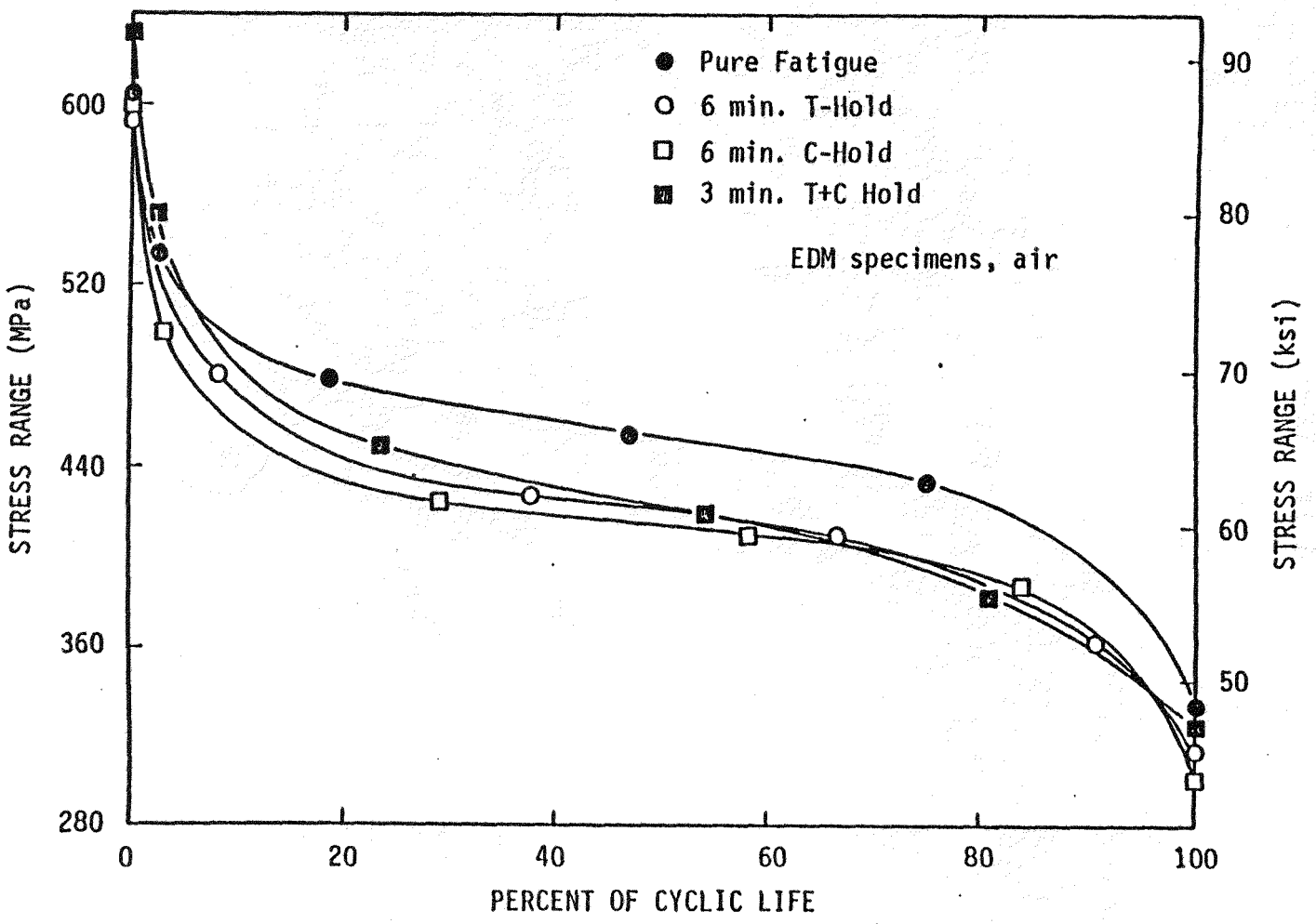

Fig. 19 Stress range versus percent of cyclic life for EDM specimens tested in air. Note the immediate softening response and also the decrease in stress range due to the hold period waveforms.

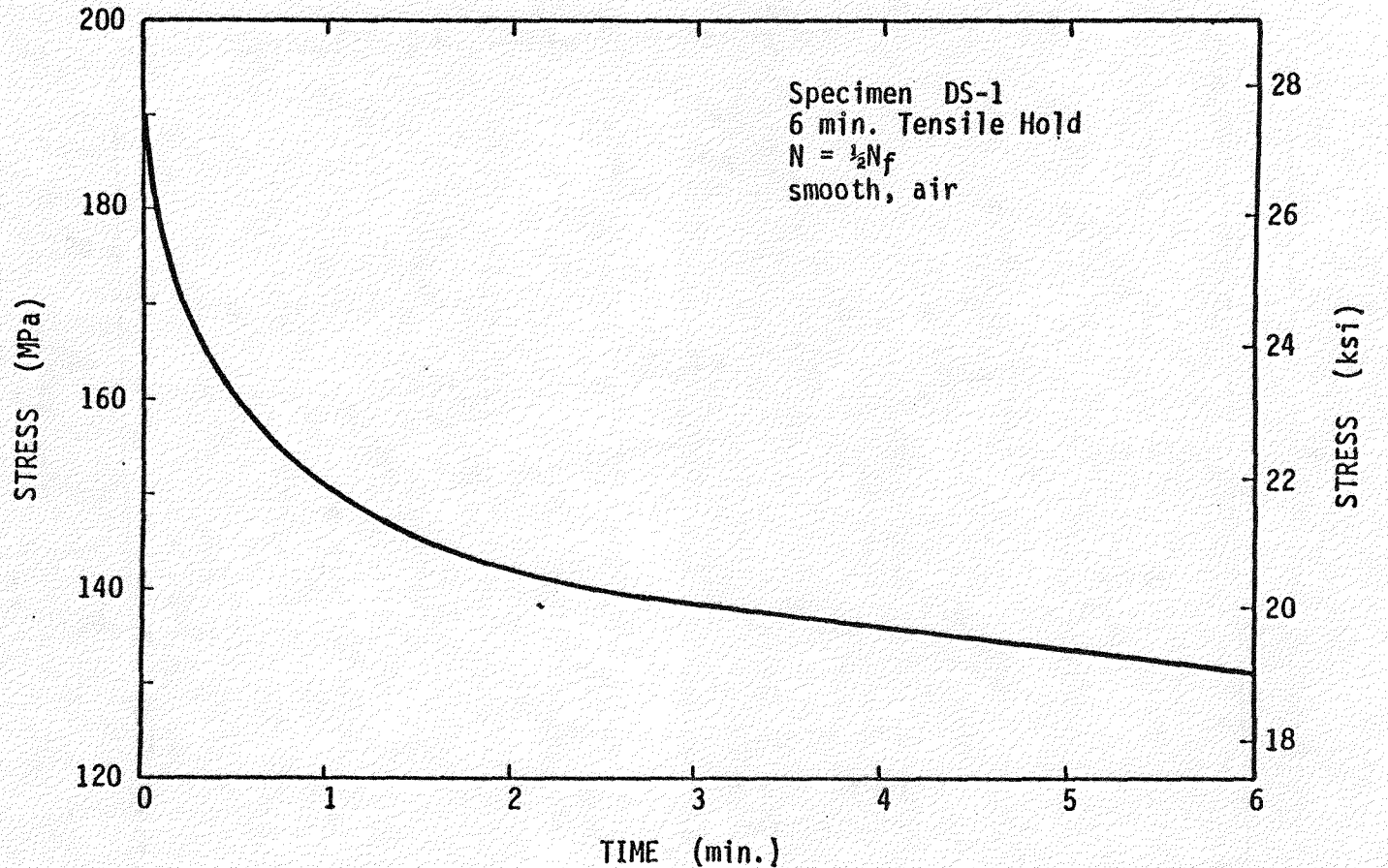

Fig. 20 Typical relaxation behavior during constant strain hold period at half the failure life. Differences between the relaxation rates in tension and compression were negligible.

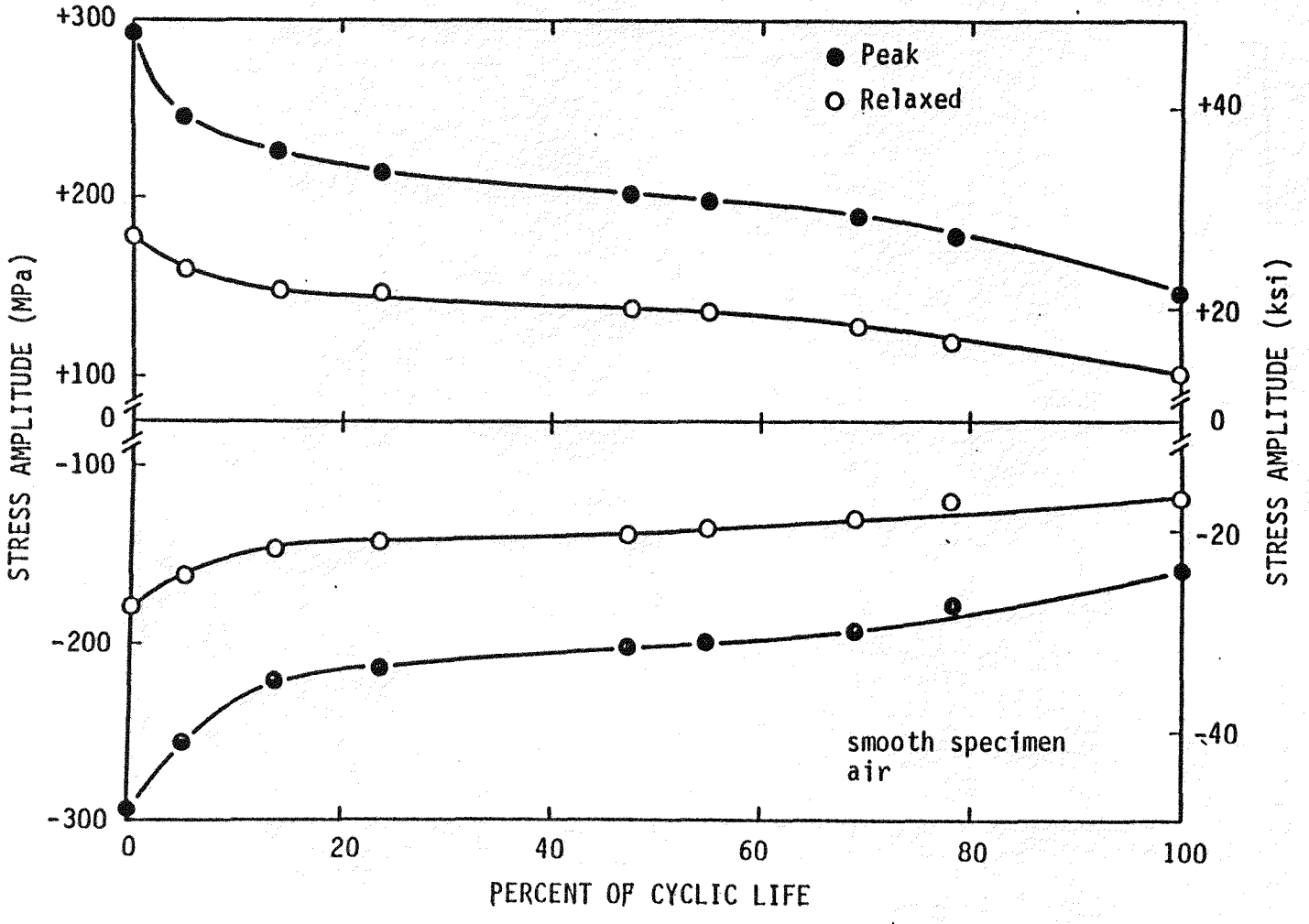

Fig. 21 Peak and relaxed stress versus percent of cyclic life showing the amount of stress relaxation throughout an entire test.

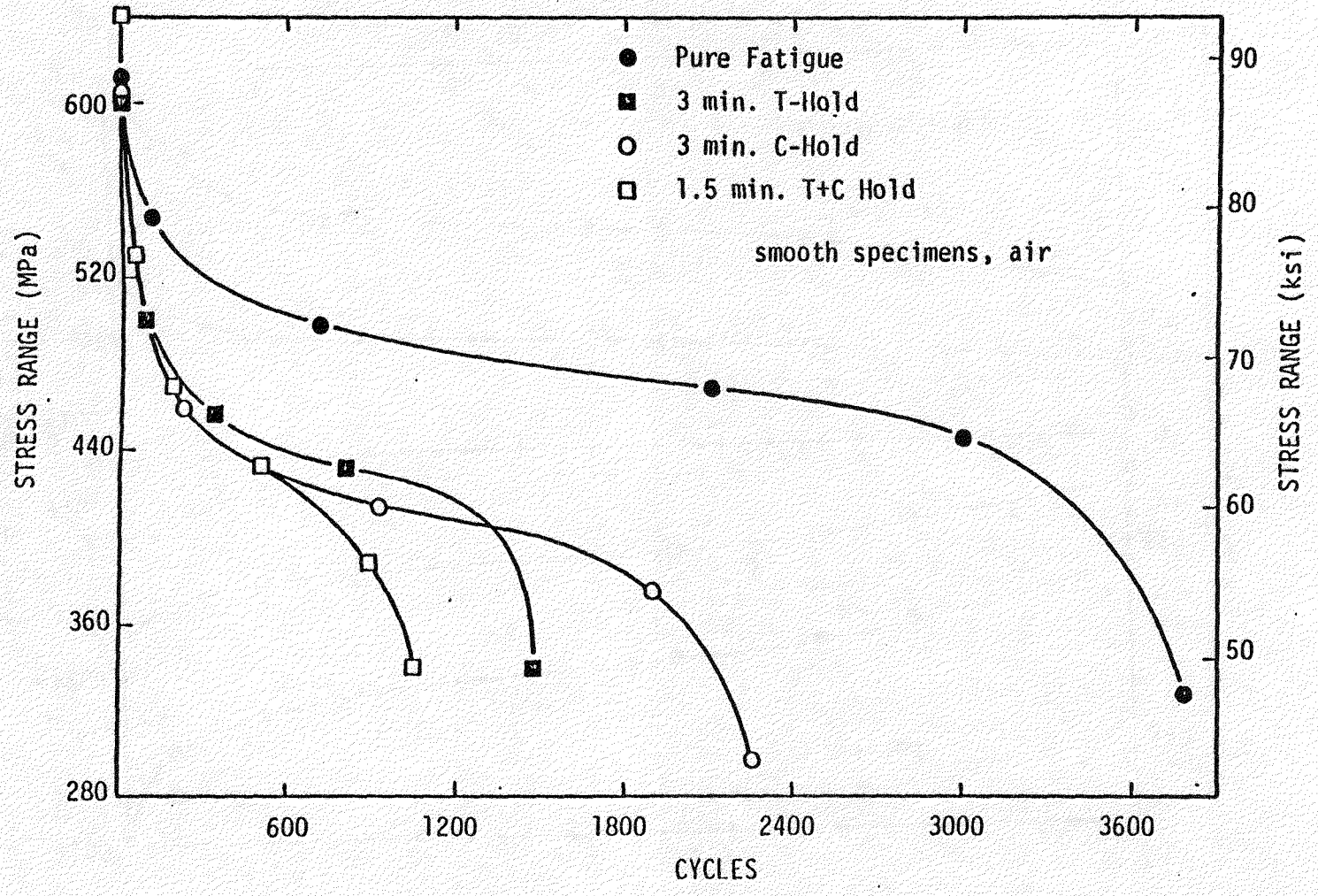

Fig. 22 Stress range versus cycles for smooth specimens tested in air indicating the deleterious effect of hold periods on fatigue resistance.

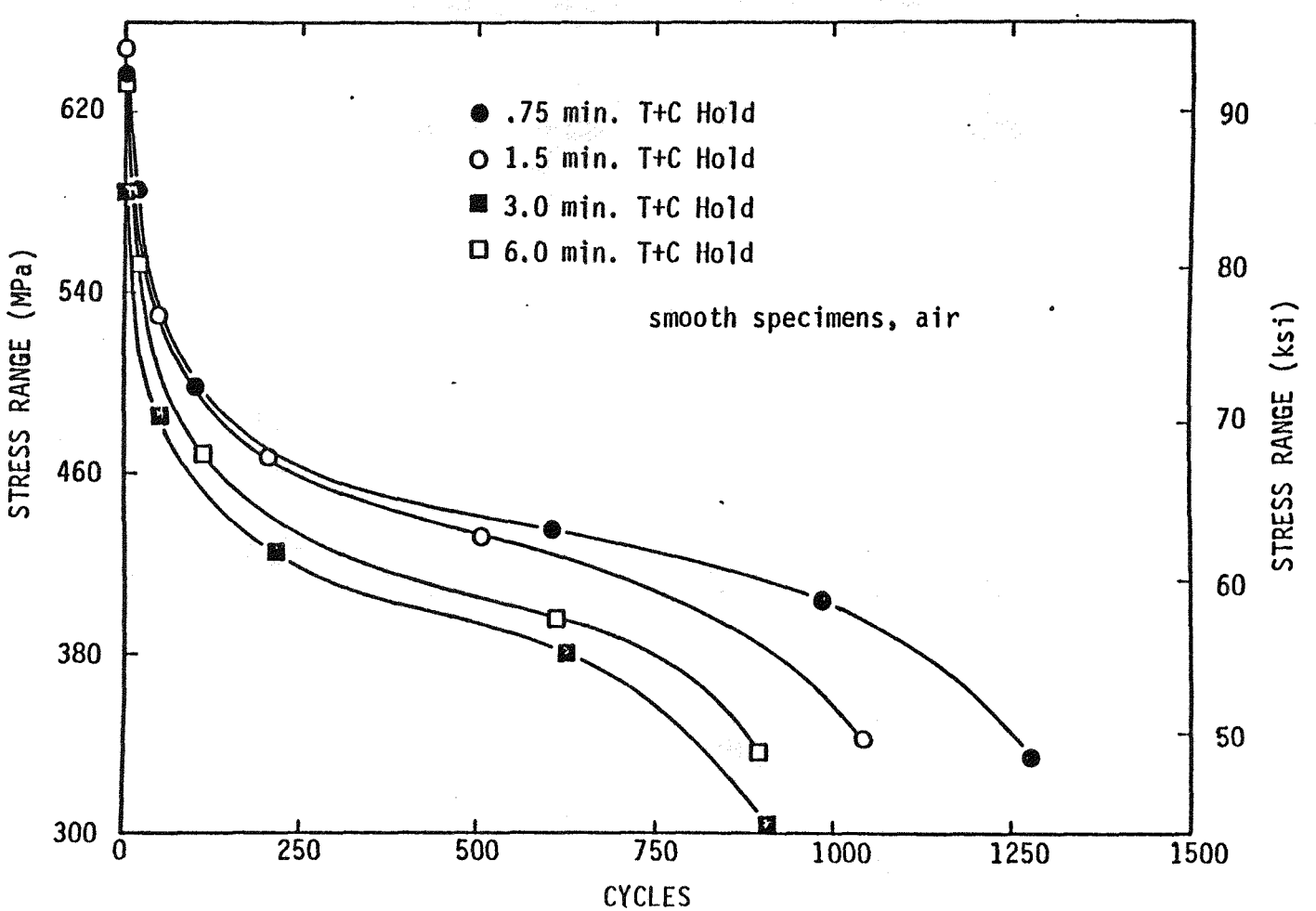

Fig. 23 Stress range versus fatigue cycles for combined tensile/compressive waveforms illustrating only minor effects of hold period duration on fatigue life.

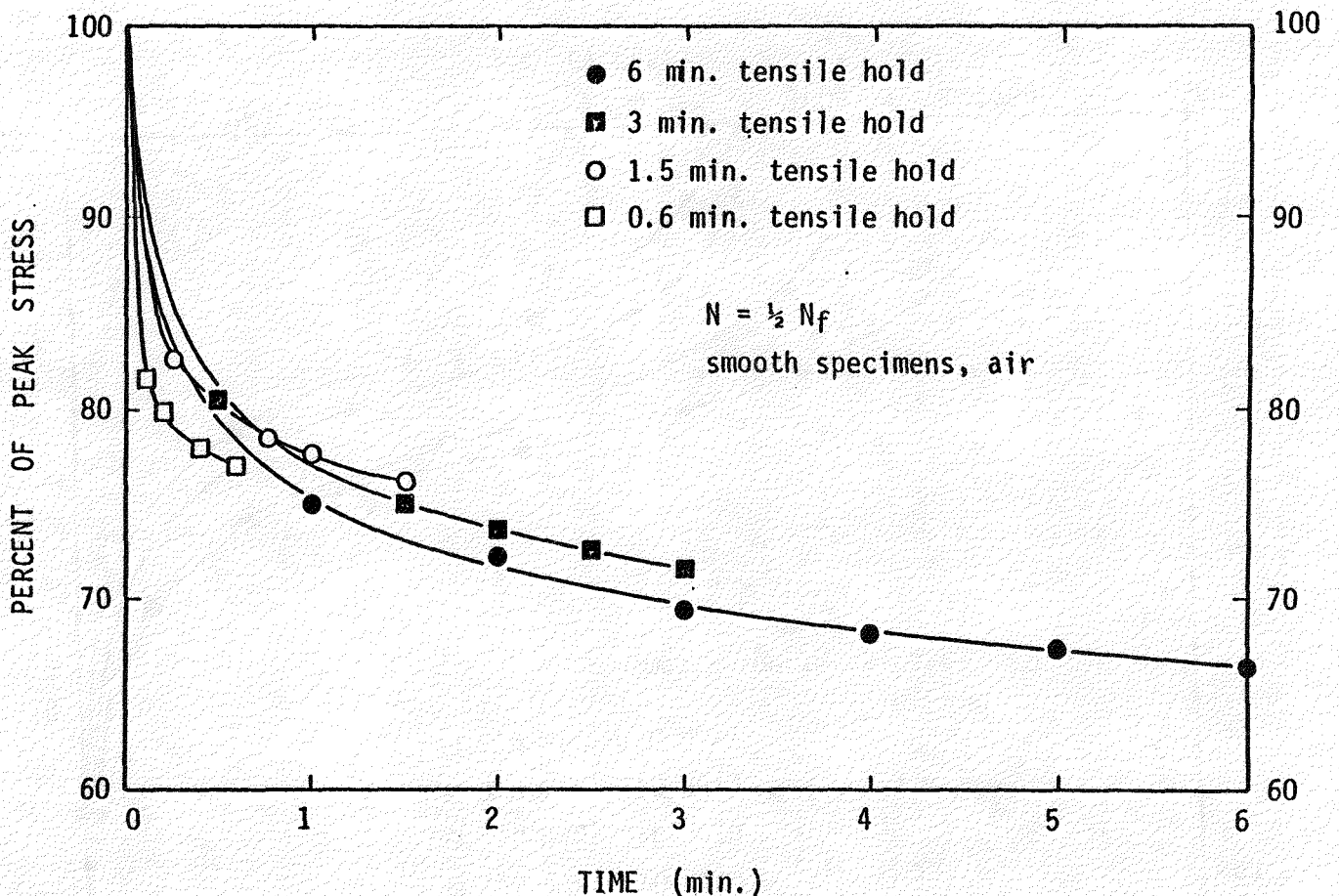

Fig. 24 Percent of peak stress versus time at half the failure life for tensile hold period waveforms with hold times ranging from 0.6 to 6 min. Note the similarity in the amount of stress relaxation in each case despite the wide variance in the hold period duration.

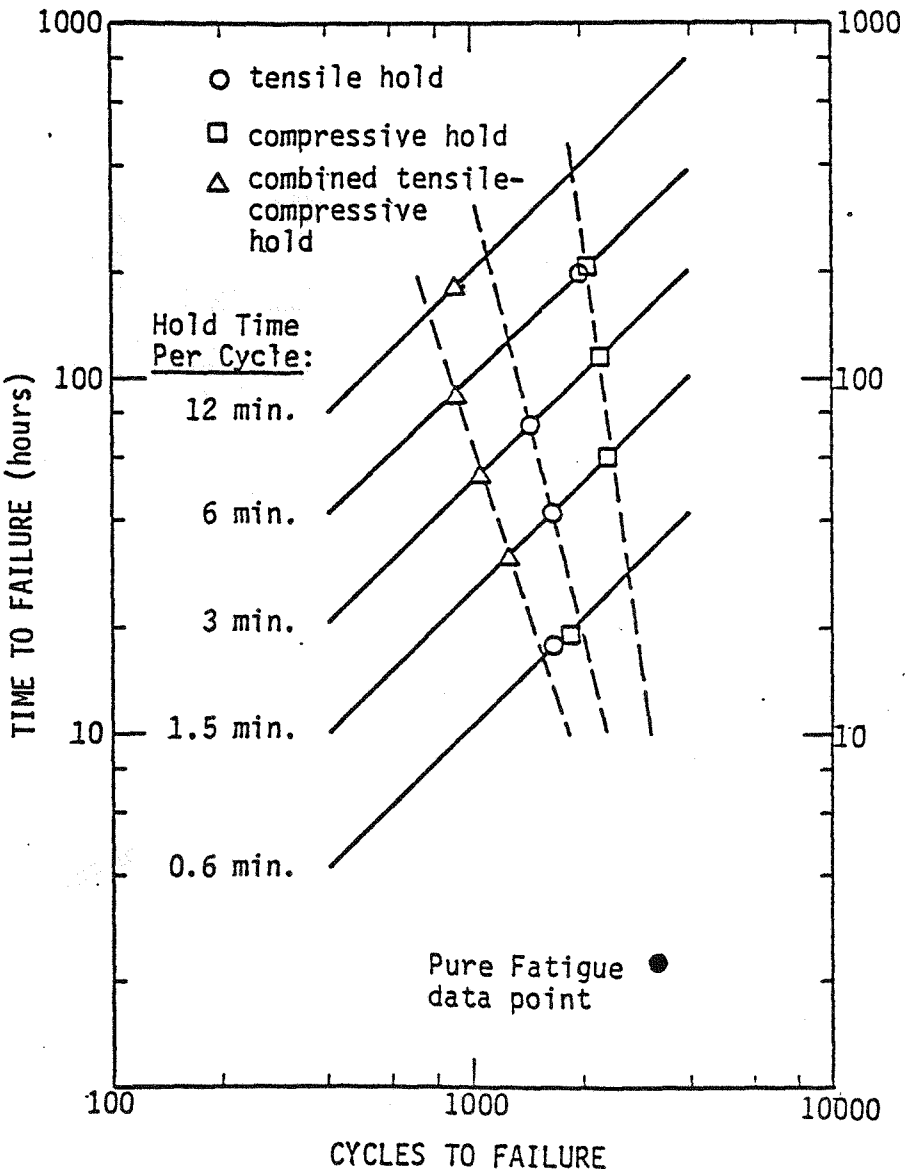

Fig. 25 Iso-strain to failure versus cycles to failure diagram showing the overall effects of hold periods.

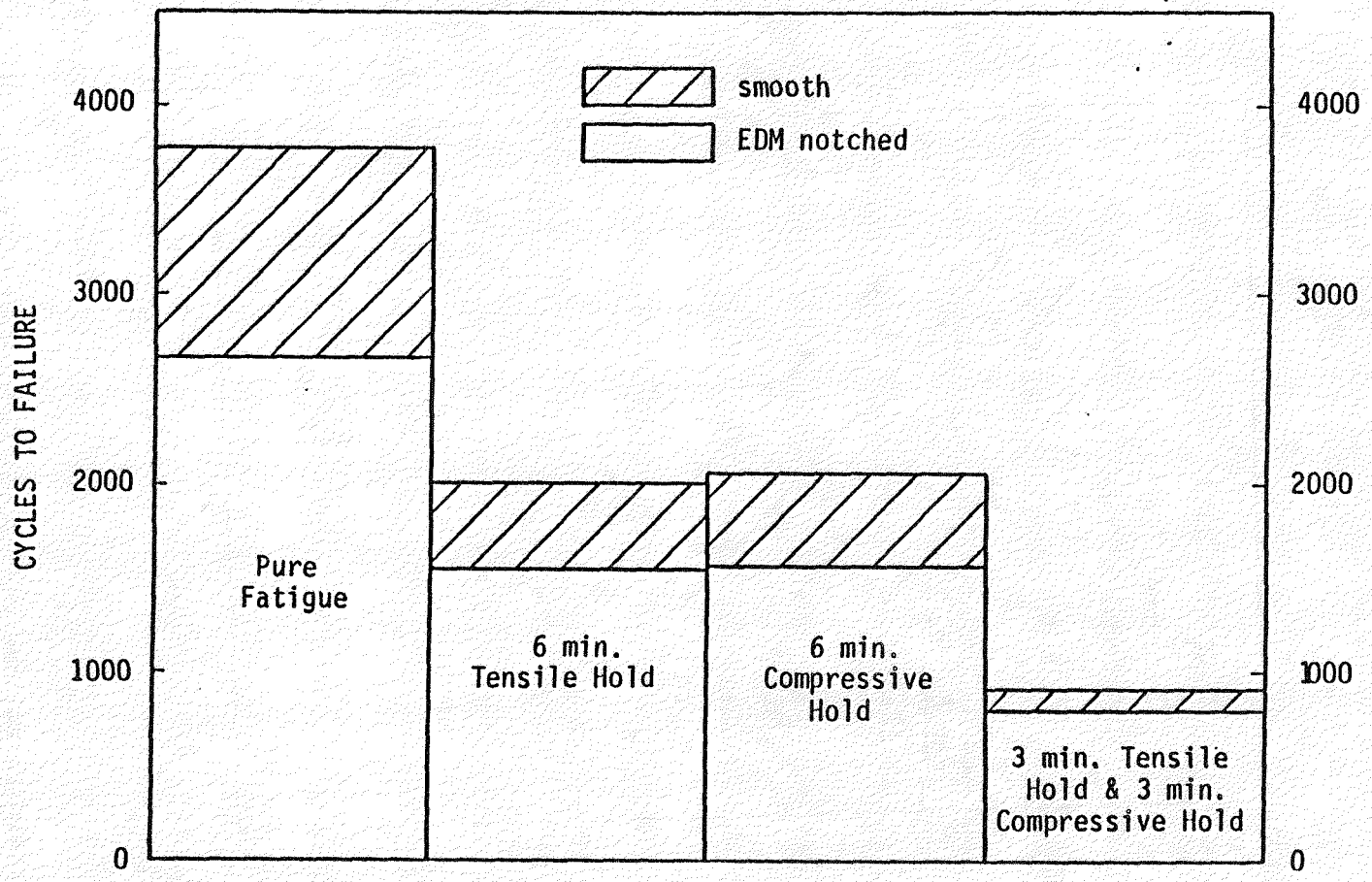

Fig. 26 Comparison of fatigue life data in air for smooth and EDM notch specimens. Average reduction in life due to EDM notches for the above waveform is 22%.

Fig. 27 Scanning electron micrograph (100X) of a typical fatigue specimen surface clearly indicating the presence of secondary crack system. The arrows indicate the loading direction.

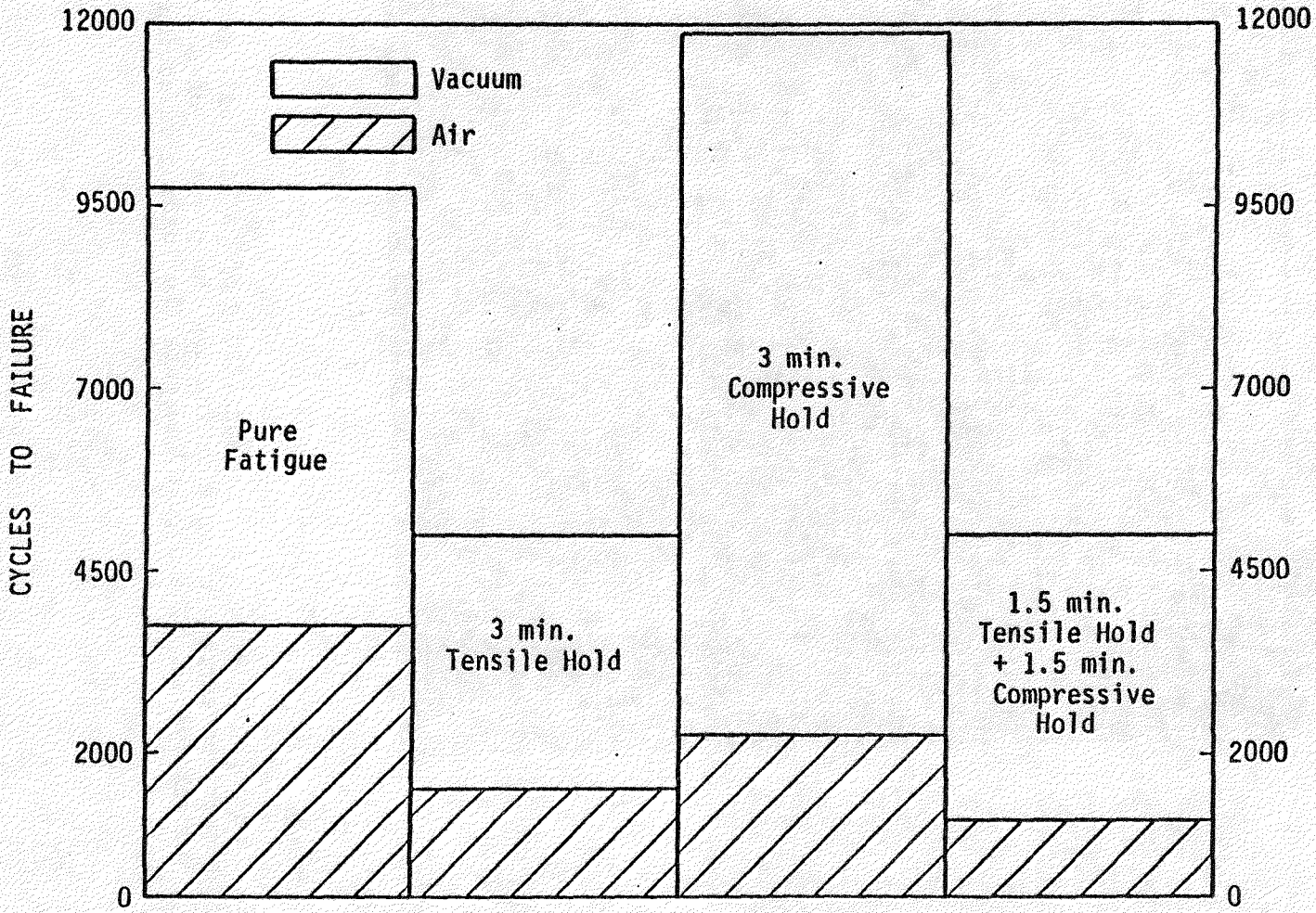

Fig. 28 Comparison of fatigue life data for smooth specimens tested in both air and vacuum. The average increase in life due to vacuum for this waveform is 410%.

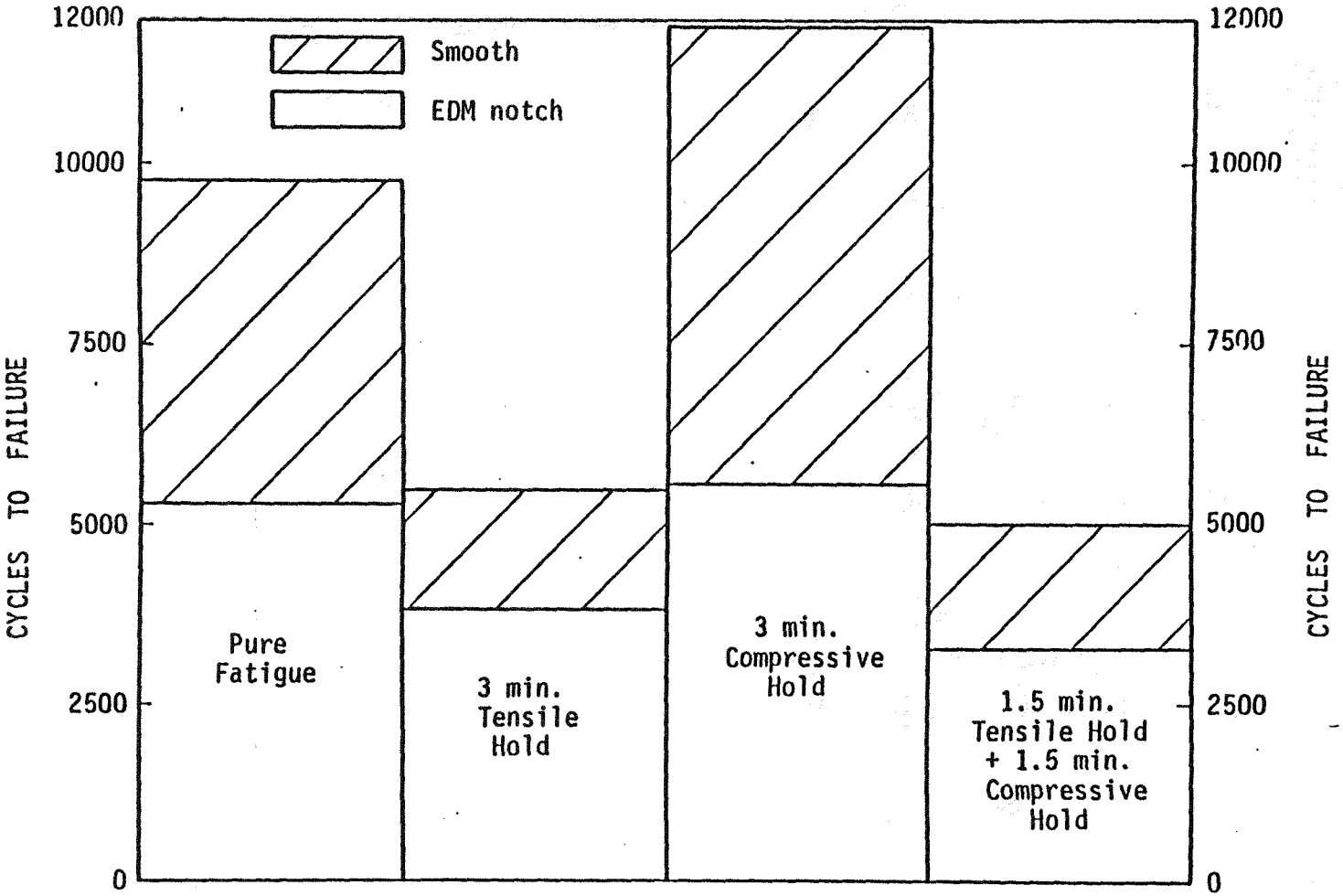

Fig. 29 Comparison of cyclic life data in vacuum for both smooth and EDM notch specimens.

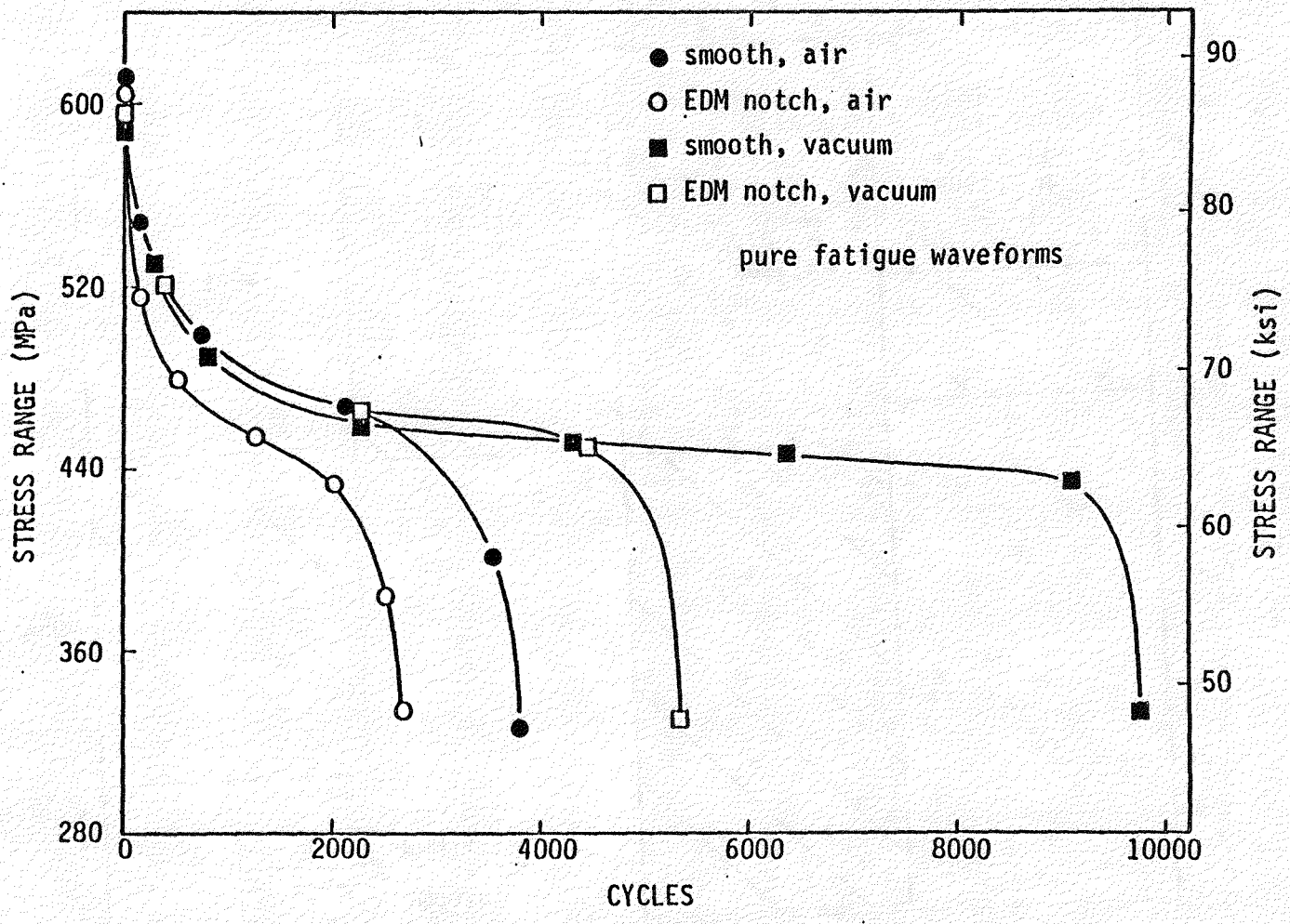

Fig. 30 Stress range as a function of cycles for pure fatigue waveforms showing the effects of smooth versus EDM notch specimen geometry and air versus vacuum.

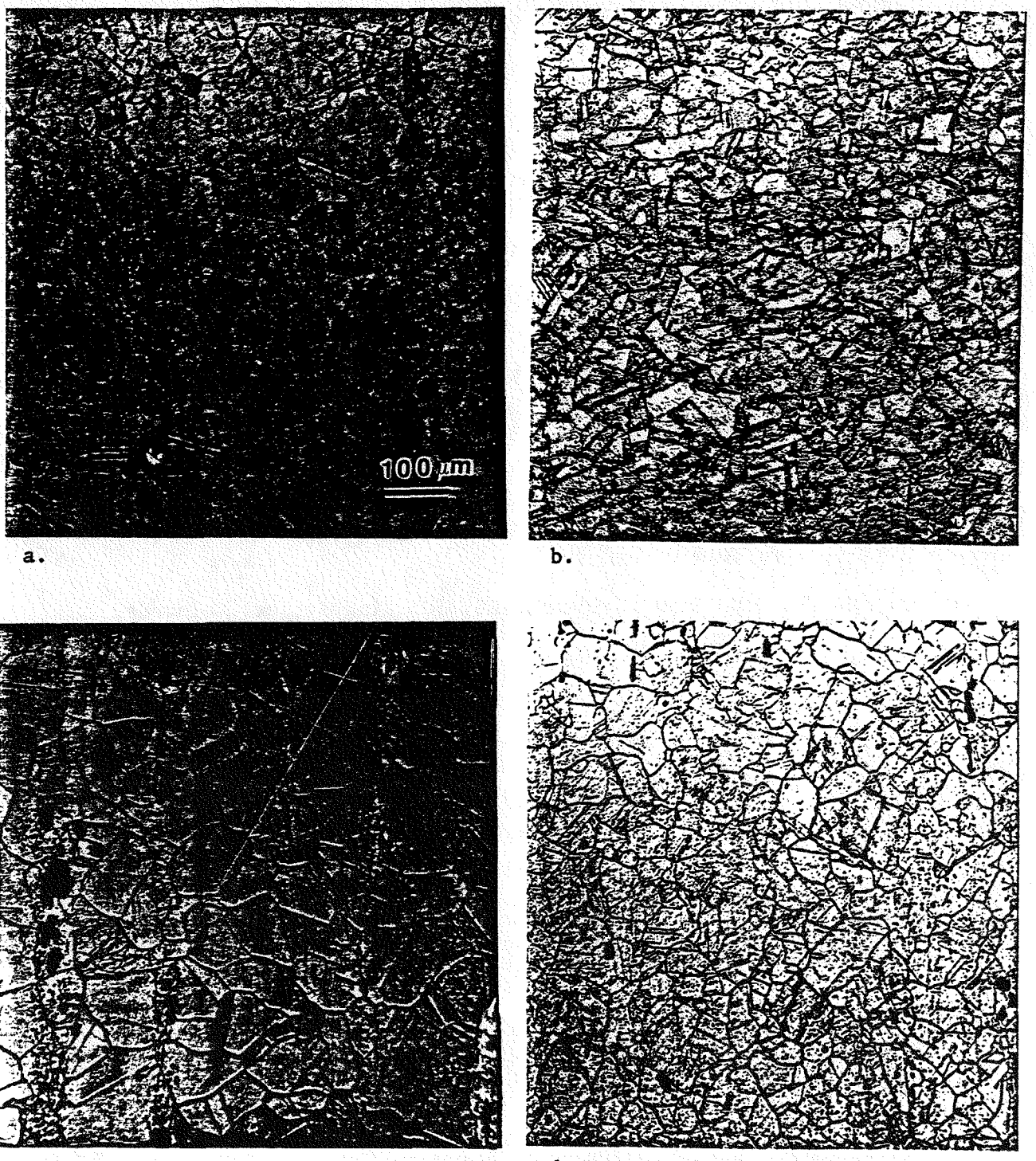

Fig. 31 Optical micrographs of the 17-14 CuMo steel forging a.) forging center, longitudinal view, b.) forging outer radius, longitudinal view, c.) forging center, transverse view, d.) forging outer radius, transverse view.

Attachment 5

1. ALLISON GAS TURBINE OPERATIONS, Mail Stop W-5, P.O. Box 420, Indianapolis, Indiana 46206

   P. Khandelwal

2. ARGONNE NATIONAL LABORATORY, 9700 S. Cass Avenue, Argonne, Illinois 60439

   W. A. Ellingson

3. AMERICAN WELDING SOCIETY, 550 LeJeune Road, Miami, Florida 33126

   H. G. Ziegenfuss

4. BABCOCK AND WILCOX, Fossil Power Generation Division, 20 South Van Buren Avenue, Barberton, Ohio 44203

   M. Gold

5. BATTELLE COLUMBUS LABORATORIES, 505 King Avenue, Columbus, Ohio 43201

   I. G. Wright

6. BETHLEHEM STEEL CORPORATION, Bethlehem, Pennsylvania 18016

   B. L. Bramfitt

7. CBI INDUSTRIES, 800 Jorie Blvd., Oak Brook, Illinois 60521

   W. R. Mikesell

8. CANADA CENTER FOR MINERAL AND ENERGY TECHNOLOGY, 555 Booth Street, Ottawa, Ontario, Canada K1A 0G1

   Mahee Sahoo

9. CHEVRON CORPORATION, P. O. Box 4012, Richmond, California 94804

   A. G. Imgram

10. CLIMAX MOLYBDENUM COMPANY OF MICHIGAN, P.O. Box 1568, Ann Arbor, Michigan 48106

    T. B. Cox

11. COLORADO SCHOOL OF MINES, Department of Metallurgical Engineering, Golden, Colorado 80401

    G. R. Edwards

12. CORNELL UNIVERSITY, Materials Sciences and Engineering Department, Bard Hall, Ithaca, New York 14853

Che-Yu Li

13. DOW CORNING CORPORATION, 3901 S. Saginaw Road, Midland, Michigan 48640

I. W. Foglesong

14. EG&G IDAHO, INC., Idaho National Engineering Laboratory, P.O. Box 1625, Idaho Falls, Idaho 83415

A. D. Donaldson

15–16. ELECTRIC POWER RESEARCH INSTITUTE, 3412 Hillview Avenue, P.O. Box 10412, Palo Alto, California 94303

W. T. Bakker
J. T. Stringer

17. FOSTER WHEELER DEVELOPMENT CORPORATION, Materials Technology Department, John Blizard Research Center, 12 Peach Tree Hill Road, Livingston, New Jersey 07039

J. L. Blough

18. GAS RESEARCH INSTITUTE, 8600 West Bryn Mawr Avenue, Chicago, Illinois 60631

H. S. Meyer

19. GIBBS & HILL ENGINEERING-DRAVO, 11 Penn Plaza, New York, New York 10001

T. A. Flynn

20. KENTUCKY CENTER FOR ENERGY RESEARCH, Iron Works Pike, P.O. Box 13015, Lexington, Kentucky 40512

V. K. Sethi

21. KENNAMETAL, INC., Philip McKenna Laboratory, 1011 Old Salem Road, P. O. Box 639, Greensburg, Pennsylvania 15601

B. North

22. LUKENS STEEL COMPANY, R&D Center, Coatesville, Pennsylvania 19320

J. A. Gulya

23. THE MATERIALS PROPERTIES COUNCIL, INC., United Engineering Center, 345 E. Forty-Seventh Street, New York, New York 10017

M. Prager

24. MOBIL RESEARCH AND DEVELOPMENT CORPORATION, P. O. Box 1026, Princeton, New Jersey 08540

R. C. Searles

25. NASA-LEWIS RESEARCH CENTER, Lewis Library, MS 60-3, 21000 Brookpark Road, Cleveland, Ohio 44135

K. Grasse

26. NATIONAL BUREAU OF STANDARDS, Materials Building, Gaithersburg, Maryland 20899

S. J. Dapkunas

27. NATIONAL MATERIALS ADVISORY BOARD, National Research Council, 2101 Constitution Avenue, Washington, DC 20418

K. M. Zwilsky

28–39. OAK RIDGE NATIONAL LABORATORY, P.O. Box X, Oak Ridge, Tennessee 37831

R. A. Bradley
P. T. Carlson
W. N. Drewery, Jr. (8)
R. R. Judkins
R. W. Swindeman

40. OFFICE OF NAVAL RESEARCH, Code 431, 800 N. Quincy Street, Arlington, Virginia 22217

S. G. Fishman

41. SHELL DEVELOPMENT COMPANY, P.O. Box 1380, Houston, Texas 77001

L. W. R. Dicks

42. THE TORRINGTON COMPANY, Research Department, 59 Field Street, Corrington, Connecticut 06790

    W. J. Chmura

43. UNITED TECHNOLOGIES RESEARCH CENTER, East Hartford, Connecticut 06108

    K. M. Prewo

44. UNIVERSITY OF CALIFORNIA AT BERKELEY, Department of Materials Science and Mineral Engineering, Berkeley, California 94720

    E. R. Parker

45. UNIVERSITY OF ILLINOIS, Department of Mechanical and Industrial Engineering, 1206 West Green Street, Urbana, Illinois 61801

    D. L. Marriott

46. UNIVERSITY OF SOUTHERN CALIFORNIA, Department of Materials Science, Los Angeles, California 90089

    J. A. Todd

47. UNIVERSITY OF TENNESSEE, Department of Chemical and Metallurgical Engineering, Knoxville, Tennessee 37916

    C. D. Lundin

48. UNIVERSITY OF WASHINGTON, Department of Materials Science and Engineering, Roberts Hall, FB-10, Seattle, Washington 98195

    J. Mueller

49. DEPARTMENT OF THE ARMY, Army Materials and Mechanics Research Center, Watertown, Massachusetts 02172

    D. R. Messier

50-52. DOE, MORGANTOWN ENERGY TECHNOLOGY CENTER, P.O. Box 880, Morgantown, West Virginia 26505

    D. Dubis
    M. Ghate
    J. S. Wilson

53. DOE, OFFICE OF FOSSIL ENERGY, Washington, DC 20545

J. P. Carr
K. N. Frye
F. M. Glaser

54. DOE, OFFICE OF BASIC ENERGY SCIENCES, Materials Sciences Division, Washington, DC 20545

F. V. Nolfi, Jr.

55. DOE, ENERGY CONVERSION & UTILIZATION TECHNOLOGIES DIVISION, Route Symbol CE-142, Forrestal Building, Washington, DC 20585

J. J. Eberhardt

56. DOE, OFFICE OF VEHICLE AND ENGINE R&D, Route Symbol CE-131, Forrestal Building, Washington, DC 20585

R. B. Schulz

57. DOE, OAK RIDGE OPERATIONS OFFICE, P.O. Box E, Oak Ridge, Tennessee 37831

E. E. Hoffman

58. DOE, PITTSBURGH ENERGY TECHNOLOGY CENTER, P.O. Box 10940, Pittsburgh, Pennsylvania 15236

S. W. Chun